Ocean acidification in the Arabian Sea and the Red Sea - factors controlling pH

by

Waleed M.M. Omer

A thesis submitted in partial fulfillment for the degree of Master of Science

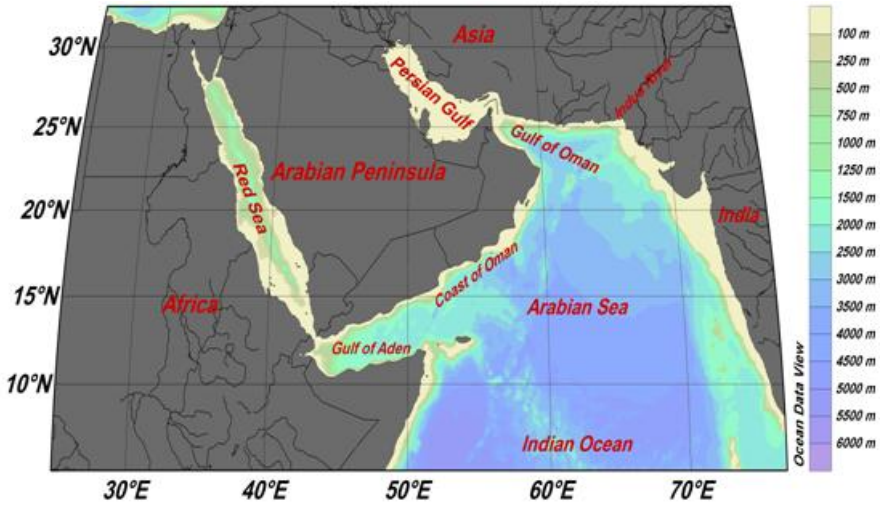

Faculty of Mathematics and Natural Sciences
Geophysical Institute
Chemical Oceanography

June 2010

UNIVERSITY OF BERGEN
Faculty of Mathematics and Natural Sciences
Geophysical Institute

Master of Science
by

Waleed M.M. Omer

Abstract

The CO_2 increase in the ocean due to uptake of anthropogenic CO_2 and the companying lowering of ocean pH is of major concern. In this study we investigated the variability of CO_2 system parameters, focusing particularly on the pH and how it changes with changes in other parameters like: temperature (T), salinity (S), total dissolved inorganic carbon (C_T), and total alkalinity (A_T). For Arabian Sea the data from the United States Joint Global Ocean Flux Study (US–JGOFS) in 1995 were used. For the Red Sea data from the Geochemical Ocean Section Study (GEOSECS) in 1977 and the Mer Rouge (MEROU) cruises in June and October 1982 were used.

The seasonal and spatial variations in pH and therefore also for calcium carbonate saturation (ΩAr for aragonite and ΩCa for calcite) are controlled by biological and physical processes that in turn are driven by the influence of monsoonal seasons. In winter season the surface average pH, ΩAr, and ΩCa in the Arabian Sea were 8.07$\pm$0.01, 3.9$\pm$0.1 and 5.9$\pm$0.2, respectively. A relatively high biological production, due to the winter cooling and mixing caused by the northeast monsoonal winds increases the pH. During summer season, Southwestern monsoonal winds caused upwelling along the coast of Oman, resulting in extremely low pH values ($\approx$7.9) and lower saturation for aragonite (ΩAr $\approx$2.36) and for calcite (ΩCa $\approx$3.62). Because of the strong change in pH, this area might serve as a natural laboratory for studies of ocean acidification.

For comparison, in the Red Sea, the surface average pH was 8.1$\pm$0.02 during winter with higher values in the north due to lower temperatures and high A_T

and C_T. The ΩAr and ΩCa were around 4.12±0.02 and 6.2±0.15, respectively, with highest values in the central part of the basin caused by higher temperatures. Summer surface pH was 8.07±0.03, with higher values in the north and the south due to relatively low temperature. In the central of the Red Sea, pH was low due to the convergence (high temperature). The ΩAr and ΩCa were averaged to 4.6±0.3 and 6.95±0.35, respectively, with higher values in the south and north. This is attributed to the high biological productivity in the south and the high temperature in the center of the Red Sea.

The vertical distributions of ΩAr, and ΩCa showed that the Arabian Sea is undersaturated with respect to aragonite below 600 m and calcite below 3500 m, whereas the Red Sea is supersaturated throughout the water column. In both seas pH was higher in the surface layers due to the consumption of CO_2 by photosynthesis, but decreased rapidly in subsurface waters due to the release of CO_2 by respiration processes. Between about 100 and 1500 m in the Arabian Sea pH is nearly constant due to the counteracting effects of decreasing temperatures and oxidation of the organic matter. The temperature effect on pH is about -0.015 units per 1°C both in the Arabian Sea and Red Sea. Thus, the 0.5°C warming reported for the Arabian Sea between 1904 and 1994, theoretically would result in a pH reduction of about 0.007, but the temporal coverage of the available data is unfortunately too short to verify this.

Acknowledgements

It is a pleasure to thank those who made this thesis possible such as my parents, who gave me the moral support, their love, encouragement and prayers.

Also I am heartily thankful to my supervisors, Truls Johannessen, Abdirahman M. Omar and Ingunn Skjelvan, their encouragement, guidance and support from the initial to the final level enabled me to develop an understanding of the subject.

I owe my deepest gratitude to the staff of the institute of marine research in Portsudan, especially their leader Dr. Abdelgadir Dafalla Elhag for encourage me to do this master study.

Lastly, I offer my regards and blessings to all of those who supported me during the completion of the project, Knut Barthel, Mahmmed A. Elfaki, my colleagues, and all the Sudanese studying and living in Bergen.

Contents

List of Figures

List of Tables

to my

Parents and every one stand with me

with my respect

Chapter 1

Aim and motivation

In the past 250 years, atmospheric carbon dioxide (CO_2) levels have increased by nearly 30% (Vitousek et al., 2008). Before the industrial revolution the level of CO_2 was approximately 280 ppmv (parts per million by volume), but at present the CO_2 level is nearly 387 ppmv, (Feely et al., 2009). This increase is driven by fossil fuel burning and deforestation. At present the atmospheric CO_2 concentration is much higher and the rate of change much faster than during the last several hundred thousands to millions of years (Raven et al., 2005). Rising atmospheric CO_2 is tempered by oceanic uptake, which accounts for nearly a third to half of anthropogenic carbon added to the atmosphere. Without the oceanic uptake the present atmospheric CO_2 would be approximately 450 ppmv (Cao and Caldeira, 2007), a level of CO_2 that would have led to even greater climate change than witnessed today. Ocean CO_2 uptake, however, is not benign; it causes increase in the concentration of hydrogen ion (H^+) and a decrease of the carbonate ion concentration (CO_3^{2-}) changing the fundamental chemical balance of the carbonate system variables in the oceans. This is commonly referred to as ocean acidification. The oceans are actually not, and probably will never become acidic. Rather, it is slightly alkaline with a global mean pH of approximately 8.16 (Figure 1.1). Thus, the term 'acidification' refers to the process of the oceans becoming less basic i.e more acidic.

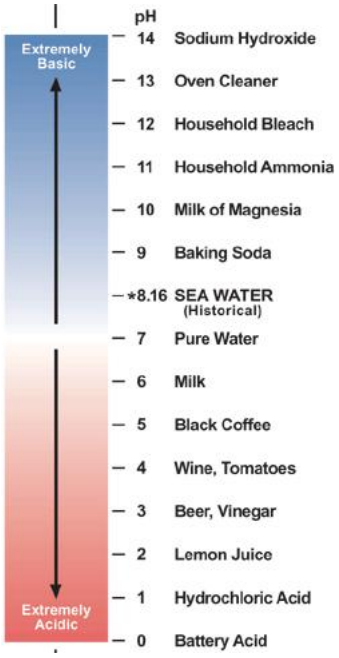

FIGURE 1.1: The pH scale which describes the acidity or alkalinity of a solution. The pH value of a solution approximates the negative logarithm (base 10) of the molar concentration of dissolved hydrogen ions (H^+). pH values of different solutions, including seawater, are shown. Figure reproduced from Feely et al. (2004).

Climate change and ocean acidification are both caused by increasing atmospheric CO_2. For this reason, acidification is commonly referred to as the "other CO_2 problem" (Henderson, 2006; Turley, 2005). Between 1750 and 2009 the surface ocean pH is estimated to have decreased from approximately 8.2 to 8.1 (Wentworth, 2009). According to Turley et al. (2007) the present pH is lower than experienced during the last 25 million years, and it will continue to decrease (Figure 1.2).

By the end of this century, we might expect a pH of about 7.6-7.8 (Orr et al., 2005) if concentrations of CO_2 emitted to the atmosphere continue to rise exponentially. That is three times greater and 100 times faster than the H^+ concentration changes seen during the climate shifts from glacial to interglacial periods (Turley et al., 2006). Even a small change in pH may lead to large changes in ocean chemistry and ecosystem functioning by changing the oceanic carbonate system, and make it difficult for the calcifying organisms, which use calcite or aragonite polymorphs of calcium carbonate to construct cell coverings or skeletons. Calcifiers span the

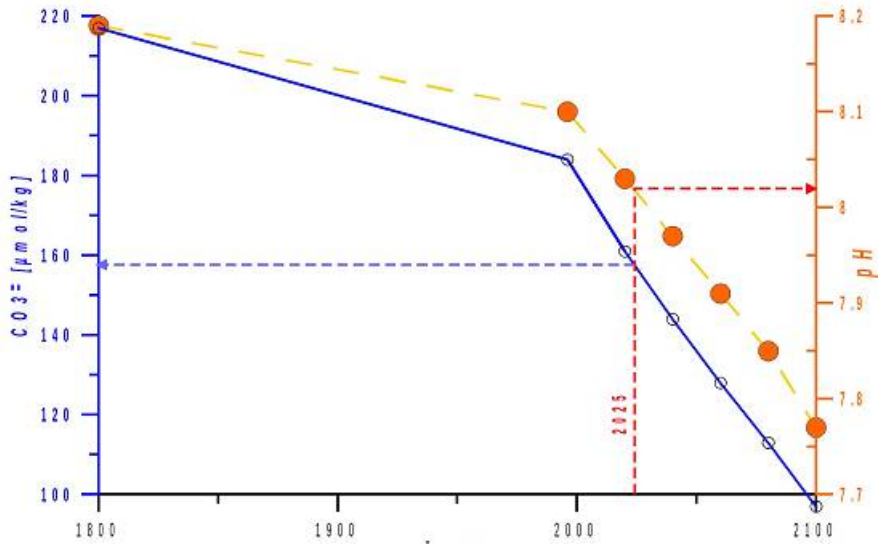

FIGURE 1.2: pH and carbonate (CO_3^{2-}) in the surface ocean between 1800 and 2100 (a global average). Values for year 1800 represent pre-industrial condition. Future scenarios are model based projections. Dashed line with red dots indicates the 2050 level, after Brewer (1997).

food chain from autotrophs to heterotrophs and include organisms such as coccolithophores, corals, foraminifera, echinoderms, crustaceans, and mollusks. Over the past 300 million years, global mean ocean pH values have probably never been more than 0.6 units lower than today (Caldeira and Wickett, 2003). Ocean ecosystems have thus evolved over time in a very stable pH environment, and it is unknown if they can adapt to such large and rapid changes which is predicted for the future.

This study focus on the Arabian Sea and Red Sea, which are two vulnerable areas in the subtropical zone. Coral reefs are well distributed along the Red Sea coast and the Arabian Sea has in general a high biological production, and these regions might be very sensitive to any change in pH.

Chapter 2

The global carbon cycle

The carbon cycle is the biogeochemical cycle which exchanges carbon, in its many forms, between the atmosphere, biosphere, oceans, and geosphere. The transport processes usually involve physical processes and chemical reactions (Figure 2.1).

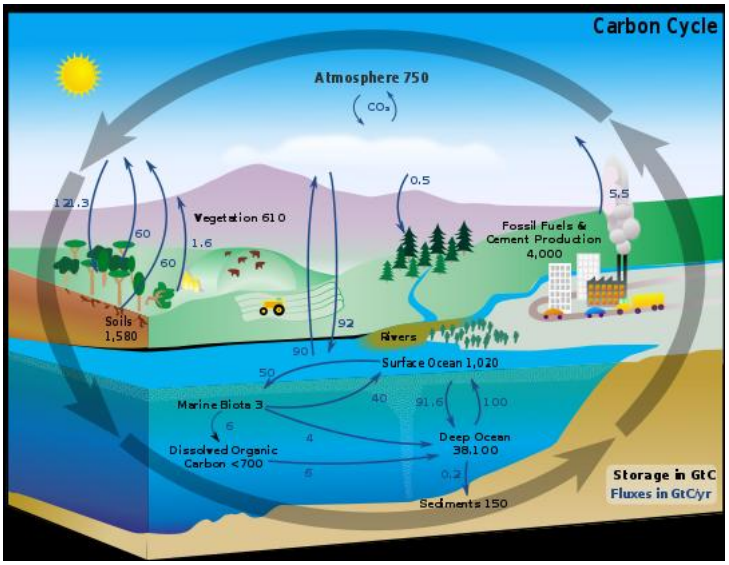

FIGURE 2.1: Diagram of the carbon cycle; the black numbers indicate how much carbon (in Gt; gigatons = 10^9 tons) are stored in the various reservoirs, the dark blue numbers indicates annual transport of carbon between reservoirs. The sediments defined in this diagram do not include the 70 million GtC of carbonate rock and kerogen. The diagram is extracted from http://en.wikipedia.org/wiki/Carbon_cycle.

There are three important carbon cycles in the earth system (Janzen, 2004):

- The short term organic carbon cycle, which emphasis on the interactions between the atmosphere and the biosphere: it has terrestrial (land) and marine (ocean) components.
- The long term organic carbon cycle, which emphasis on the formation and destruction of fossil fuels and other sediments containing organic carbon.
- The inorganic carbon cycle which emphasis on calcium carbonate, by far the largest of the carbon reservoirs.

On land carbon is cycled primarily as CO_2 in living biota and as decaying organic matter. In the ocean the main form of carbon is bicarbonate (HCO_3^-), and the atmosphere act as a strong link between the land and the ocean.

The largest carbon reservoir is the deep ocean, which contains about 40,000 Gt C (Gt = 10^9 tons). In contrast the land contains 2,000 Gt C, the atmosphere 750 Gt C, and the upper ocean 1,000 Gt C (Figure 2.1) (Janzen, 2004). The concentration of CO_2 in the ocean follows Henry's law which states that an increase in the atmospheric CO_2 concentration leads to increase in the surface ocean concentration through absorbing more CO_2.

CO_2 is an un-reactive gas in the atmosphere, but when it is absorbed by the ocean (Eq. 2.1), due to difference in partial pressure between the atmosphere and the ocean, it becomes reactive and takes part in several chemical, physical, biological, and geological reactions;

$$CO_{2(atomosphere)} \longrightarrow CO_{2(dissolved)} \tag{2.1}$$

CO_2 reacts with water to produce carbonic acid (H_2CO_3);

$$CO_{2(dissolved)} + H_2O \longrightarrow H_2CO_3 \tag{2.2}$$

H_2CO_3 dissociates and releases hydrogen ions into the water;

$$H_2CO_3 \longrightarrow HCO_3^- + H^+ \tag{2.3}$$

Ionization of the bi-carbonate (HCO_3^-) releases the carbonate ion (CO_3^{2-});

$$HCO_3^- \longleftrightarrow H^+ + CO_3^{2-} \tag{2.4}$$

These reactions (Eq. 2.2, 2.3, 2.4) are very rapid, on time scales of tens of seconds for CO_2 hydration and microseconds for subsequent acid-base reactions (Dickson et al., 2007; Zeebe and Wolf-Gladrow, 2001). The amount of CO_2, HCO_3^-, and CO_3^{2-} concentrations determines the pH of the seawater, as shown in Figure 2.2.

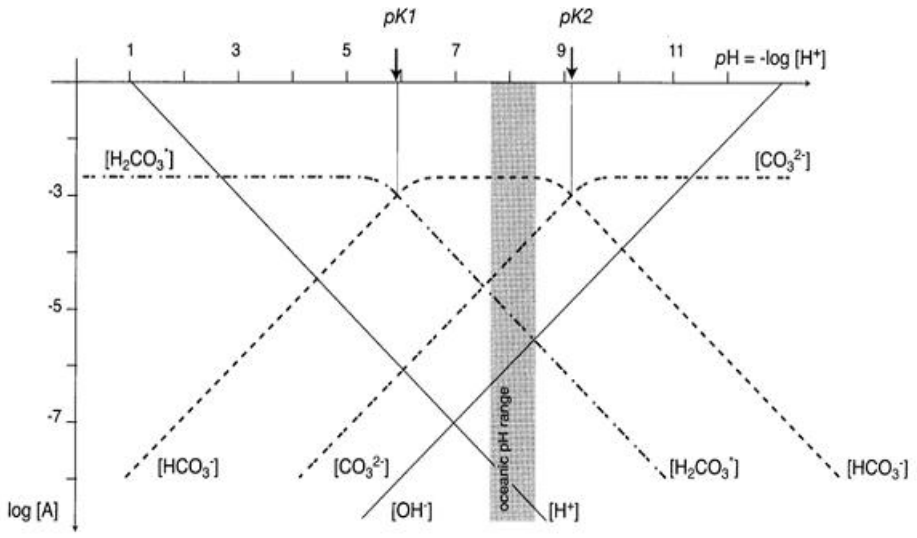

FIGURE 2.2: Concentration of the different inorganic carbon species as a function of pH. Note that the vertical axis is logarithmic (base 10); Figure from Sarmiento and Gruber (2006).

In the ocean, calcifying organisms combine carbonate with calcium to form calcium carbonate ($CaCO_3$) according to:

$$CaCO_3 \longleftrightarrow Ca^{2+} + CO_3^{2-} \tag{2.5}$$

Owing to this biological process, limestone is the largest reservoir of carbon in the carbon cycle. The calcium comes from weathering of calcium-silicate rocks, which causes the silicon in the rocks to combine with oxygen to form sand or quartz (silicon dioxide), leaving calcium ions available to form limestone.

As depicted in Figure 2.3, several chemical, physical and biological factors have the potential to affect the uptake of CO_2 by the ocean. Furthermore, carbon is transported between surface and sub-surface ocean by different processes. The solubility

pump is one of these processes and that describes the absorption/release of carbon from/to the atmosphere due to decreasing/increasing seawater temperatures. The solubility of carbon dioxide is a strong inverse function of seawater temperature, and gas solubility is greater in cold water than in warm water. Decreasing temperature and increasing salinity at high latitudes forms dense water, rich in carbon, which sinks and drives the thermohaline circulation. This process transports CO_2 from the high latitudes (low temperature - dense water) to the warm equatorial region (high temperature) where CO_2 is degassed to the atmosphere due to low gas solubility and upwelling of the deep water, so the equatorial waters are supersaturated with respect to CO_2. Circulation makes sure that CO_2 is constantly being exchange between the ocean and the atmosphere. The re-equilibration time for CO_2 is slow (typically several months) due to the dissociation of CO_2 in seawater (Dickson et al., 2007). The observation that the net oceanic uptake of anthropogenic CO_2 is only about 2% of the total CO_2 cycled annually across the air-sea interface ought to be of major concern; the significant perturbations arising from this small change in flux imply that the system is extremely sensitive. Any resulting changes in the biogeochemistry of the mixed layer could have a major impact on the magnitude (or even sign) of the total CO_2 flux and hence on the Earth's climate.

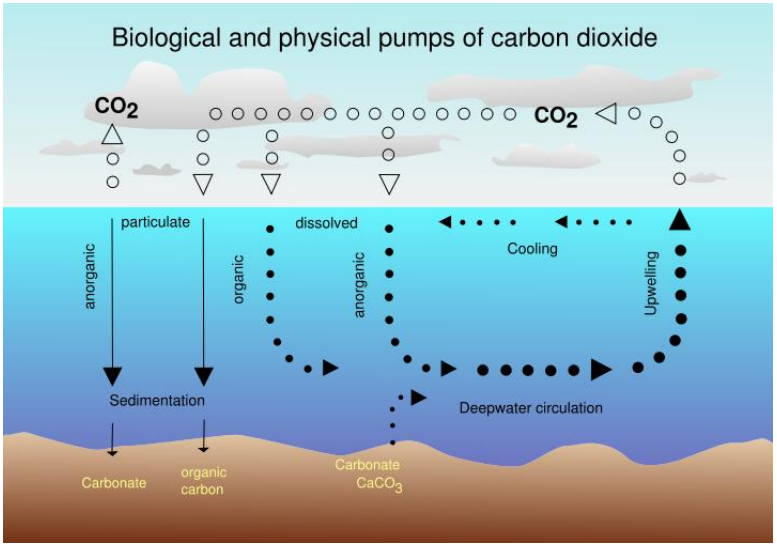

FIGURE 2.3: Biological and physical pumps of carbon dioxide http://en.wikipedia.org/wiki/File:CO2_pump_hg.svg.

The other important mechanism is the biological pump which describes a suite of biological- mediated processes which transport carbon from the surface euphotic zone to the ocean interior. Ocean organisms growth consumes dissolved carbon dioxide (CO_2) in the surface seawater. Depending on the base line pCO_2 this might cause an undersaturation of dissolved CO_2 and uptake from the atmosphere. Organisms within the surface ocean exchange CO_2 in much the same way as the biological processes on land by a process called photosynthesis;

$$6CO_2 + 6H_2O \longleftrightarrow C_6H_{12}O_6 + 6O_2 \tag{2.6}$$

CO_2 is released to the atmosphere by respiration and those activities are in near balance. Although the biological uptake of CO_2 per unit area of the surface oceans is lower than that in most terrestrial systems, the overall biological absorption is almost as large as that in terrestrial environment, because the surface area of the oceans is much larger (Field et al., 1998). When plankton dies it sinks and remineralize, and inorganic carbon is returned into the water, either at the seafloor or somewhere in the water column, (Figure 2.3). Mixing processes, such as upwelling, returns the remineralized inorganic carbon to the surface water and this causes a decrease in pH, see Figure 2.4.

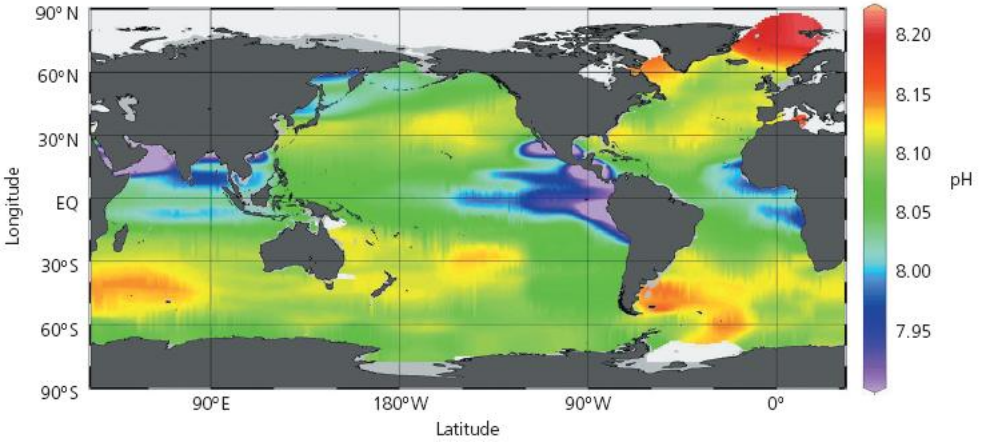

FIGURE 2.4: pH values of the mixed surface layer (upper 50 m) in the global ocean in 1994, the pH is lower in the upwelling regions (Raven et al., 2005).

Investigations of the marine carbon cycle are usually conducted through determinations of four variables; total dissolved inorganic carbon, total alkalinity, partial pressure of CO_2, and pH.

Total dissolved inorganic carbon (C_T) is defined as the sum of all carbon species dissolved in seawater i.e. bicarbonate (HCO_3^-), carbonate (CO_3^{2-}), and CO_2 (Zeebe and Wolf-Gladrow, 2001);

$$C_T = [CO_2^*] + \left[HCO_3^-\right] + \left[CO_3^{2-}\right] \tag{2.7}$$

where CO_2^* is the sum of carbon dioxide and carbonic acid (H_2CO_3) in the ocean. C_T varies due to various processes such as air-sea gas exchange, biological production and decay, and also C_T decreases slightly due to the formation of the $CaCO_3$ and increase upon the dissolution, see Figure 2.5.

Total alkalinity (A_T) is the total concentration of bases in water expressed as micro equivalents per kg (μEq kg^{-1}) or micromole per kg (μmol kg^{-1}). These bases are usually bicarbonates (HCO_3^-) and carbonates (CO_3^{2-}), and they act as a buffer system that prevents drastic changes in pH (Zeebe and Wolf-Gladrow, 2001);

$$\begin{aligned} A_T = &\left[HCO_3^-\right] + 2\left[CO_3^{2-}\right] + \left[B(OH)_4^-\right] + \left[OH^-\right] + \left[HPO_4^{2-}\right] + 2\left[PO_4^{3-}\right] \\ &+ \left[SI(OH)_3^-\right] + [NH_3] + \left[HS^-\right] - \left[H^+\right]_F - \left[HSO_4^-\right] - [HF] - [H_3PO_4] \end{aligned} \tag{2.8}$$

Alkalinity is mainly influenced by salinity variations (high salinity high A_T), in addition to calcium carbonate formation (decreasing A_T) or dissolution (increasing A_T). A_T is only slightly affected by production of particulate organic matter through the hydrogen ion consumed during photosynthesis, and increases slightly due to photosynthesis and decreases due to respiration (Figure 2.5). Total alkalinity is lower in surface water than the deep water, because it is reduced by the surface calcification process.

Partial pressure of CO_2 (pCO_2) or fugacity of CO_2 (fCO_2) is the concentration of CO_2 in dry air at equilibrium with the ocean divided by the solubility of CO_2 in seawater; it varies with latitude (Zeebe and Wolf-Gladrow, 2001). There are three processes which cause change in pCO_2 (Honda et al., 1997):

- Change in CO_2 solubility depending on water temperature and salinity (Solubility pump); low temperature leads to high solubility and vice versa.

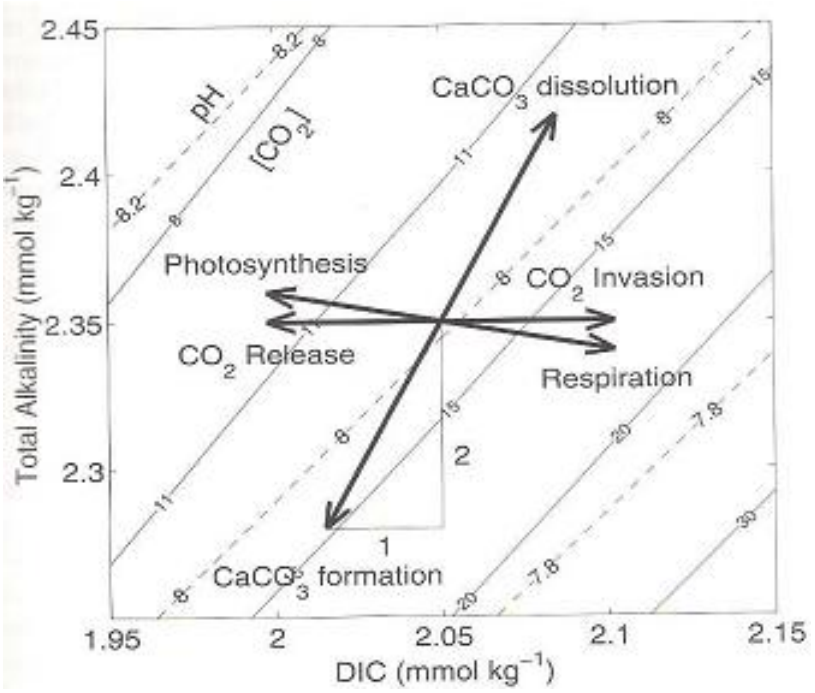

FIGURE 2.5: Effect of various marine processes on C_T and A_T, from Zeebe and Wolf-Gladrow (2001).

- Change in alkalinity caused by $CaCO_3$ formation or dissolution (Alkalinity pump); pCO_2 increase when $CaCO_3$ is formed (calcification), and decrease when it dissolves.
- Change in total dissolved carbon caused by the formation of organic matter (Biological pump); pCO_2 decreases when organic matter is formed and increases when it decays.

fCO_2 differs from pCO_2 in that it takes account of the non-ideal nature of the gas phase (Dickson et al., 2007). The fugacity of a gas such as CO_2 can be determined from knowledge of its equation of state;

$$fCO_2 = pCO_2 \exp(P\frac{B + 2\delta}{RT}) \tag{2.9}$$

where fCO_2 and pCO_2 are in μatm. P = the total atmospheric pressure in Pa (1 atm = 101325 Pa).

B = the first virial coefficient of CO_2 in m^3 mol^{-1}.

δ = the cross virial coefficient in m^3 mol^{-1}.

R = 8.314 J K^{-1} mol^{-1} is the gas constant.

T = the absolute temperature in Kelvin.

The first virial coefficient (B) has been determined by Weiss (1974);

$$B = \left(-1636.75 + 12.0408T - 3.27957 \times 10^{-2}T^2 + 3.16528 \times 10^{-5}T^3\right) 10^{-6} \tag{2.10}$$

The cross virial coefficient is defined as

$$\delta = (57.7 - 0.118T)10^{-6} \tag{2.11}$$

pH is defined as the negative logarithm of total hydrogen ions concentration $[H^+]_T$ in mole per kg seawater;

$$\mathrm{pH} = -\log\left[H^+\right] \tag{2.12}$$

It is primarily affected by primary production, respiration, air-sea CO_2 exchange, and $CaCO_3$ formation and dissolution (Figure 2.5). Distinct pH scales exist depending on the method of determination:

The NBS (National Bureau of Standards) pH scale, pH_{NBS}, make use of several standard buffer solutions with assigned pH values. Unfortunately, the ionic strength of the standard solutions are much lower (≈0.1 M) than that of seawater (≈0.7 M). This causes large changes in the liquid junction potential between standards and sample, and introduces errors larger than the required accuracy in pH. For this reason, the pH_{NBS} scale is not recommended for use with seawater pH determinations (Zeebe and Wolf-Gladrow, 2001).

The free pH scale, pH_F, takes into account the sulphate ion concentration in seawater, and the total concentration of H^+, $[H^+]_T$, is defined as

$$\left[H^+\right]_T = \left[H^+\right]_F + \left[HSO_4^-\right] \tag{2.13}$$

where $[H^+]_F$ refers to the free H^+ ions. Analytically, only $[H^+]_T$ can be determined (Dickson, 1984), and $[H^+]_F$ can then be calculated from Eq. 2.13 using the dissociation constant for sulphate. The utility of this scale is limited by the complexity of an accurate determination of sulphate dissociation constant. pH_F values differ by up to 0.12 pH units from both the total and seawater scales.

The total pH scale (Hansson, 1973), denoted by pH_T, was defined using buffer standard solutions based on synthetic seawater, which eliminated the problem of different ionic strength. This pH scale is defined as

$$pH_T = -\log \left[H^+\right]_F \tag{2.14}$$

where the effect of the sulphate dissociation constant is included in the $[H^+]_T$ relation (see Eq. 2.13). In this work, pH total scale is used, see Chapter 6.

The seawater pH scale, pH_{SWS}, also takes into account the fluoride ions in solution:

$$H^+ + F^- \longleftrightarrow HF \tag{2.15}$$

and $[H^+]_T$ is the sum of $[H^+]_F$, $[HSO_4^-]$, and [HF]. However, the concentration of sulfate ions is much larger than the concentration of fluoride, so the difference between the total and seawater scales is very small.

Measuring any two of the four primary parameters, C_T, A_T, pH, or pCO_2, allows for the determination of the other two carbon parameters and a wide range of pH dependent species.

Chapter 3

Chemistry of carbonate minerals

As mentioned in the previous chapter, CO_2 dissolves in the water and forms carbonic acid (H_2CO_3) which dissociates quickly in the water and release H^+ (Eq. 2.3). The increase in the number of the hydrogen ions leads to an increase in acidity i.e. a decrease in pH. Some of these hydrogen ions react with carbonate ions to form bicarbonate:

$$H^+ + CO_3^{2-} \longrightarrow HCO_3^- \tag{3.1}$$

Thus, the net effect of the dissolution of CO_2 in seawater is to increase concentration of H^+, H_2CO_3 and HCO_3^-, while decreasing concentration of CO_3^{2-}. Carbonate ions are used by many marine organisms to build their skeletons which combine Ca^{2+} and CO_3^{2-} to form shells of calcium carbonate ($CaCO_3$) according to Eq. 2.5. Calcium carbonate exists in three forms with different crystalline structure. Calcite is the least sensitive to acidification (low solubility in sea water) whereas aragonite and high-Mg calcite are especially sensitive to acidification (more soluble in sea water than calcite).

The decreasing concentration of CO_3^{2-}, due to oceanic absorption of CO_2 hampers the formation of carbonate minerals and promoting their dissolution. The latter process provides carbonate ions that can consume H^+ according to Eq. 3.1. Thus, the dissolution of carbonate minerals tends to decrease $[H^+]$ (increase pH) counteracting some of the pH effects of added CO_2. Therefore, the reaction of H^+

and CO_3^{2-} to form HCO_3^- (Eq. 3.1) is termed the carbonate buffer to describe how the dissolved inorganic carbon system in seawater acts to diminish changes in ocean H^+ concentration, and thus pH. Because of this buffering, the change in pH resulting from CO_2 addition is much less than it would be without inorganic carbon species in the ocean. But this process also consumes some carbonate ions; therefore this pH buffering capacity would diminish as CO_2 concentrations increases. Since CO_2 is absorbed at the sea surface; it is the surface oceans that are most affected and the diminishing of buffering is readily observable.

At time scales of ocean mixing, interaction with $CaCO_3$-rich sediments tends further to buffer the chemistry of the seawater so that changes in pH are diminished. For example, if the deep oceans start to become more acidic, the concentration of CO_3^{2-} will decrease and some carbonate ion will be dissolved from the sediments. Because $CaCO_3$ is abundant in sediments, the pH of the deep oceans cannot change by large amounts over timescales of 10.000 years (Sarmiento and Gruber, 2006). However, a significant change of 0.1 pH units in surface waters has already been observed since the industrial revolution, according to Orr et al. (2005).

In open ocean waters small organisms with shells of $CaCO_3$ fall to the seafloor upon death. Their preservation in the sea floor sediments depends on the solubility of $CaCO_3$ in seawater and on the concentration of carbonate ions. The product of Ca^{2+} concentrations and CO_3^{2-} in equilibrium with mineral $CaCO_3$ is a constant called the apparent solubility product (K_{sp}). Equations for K_{sp} with respect of calcite and aragonite can be found in Sarmiento and Gruber (2006) and it varies with temperature, salinity and pressure, and differs among the $CaCO_3$ minerals. The solubility product and the concentrations of Ca^{2+} and CO_3^{2-} are used to define the degree of saturation of $CaCO_3$ minerals phases (Ω) according to:

$$\Omega = \frac{\left[Ca^{2+}\right]\left[CO_3^{2-}\right]}{K_{sp}} \tag{3.2}$$

Another useful quantity is the saturation state which is the difference between the observed CO_3^{2-} ion concentration and the saturation CO_3^{2-} concentration (Sarmiento and Gruber, 2006);

$$\Delta CO_3^{2-} = \left[CO_3^{2-}\right] - \left[CO_3^{2-}\right]_{saturated} \tag{3.3}$$

Because added CO_2 decreases the carbonate ion concentration, the saturation horizons will become shallower with increasing amounts of human-derived CO_2 released to the atmosphere. At present, the marine organisms that produce $CaCO_3$ shells live above the saturation horizon, where $CaCO_3$ does not really dissolve, but this situation might change in the future due to the ocean acidification which will tend to release more H^+ in the ocean (Orr et al., 2005). In general, the cold Southern Ocean is particularly vulnerable to changes in saturations levels because it currently has very shallow saturation levels (Orr et al., 2005), see Figuer 3.1.

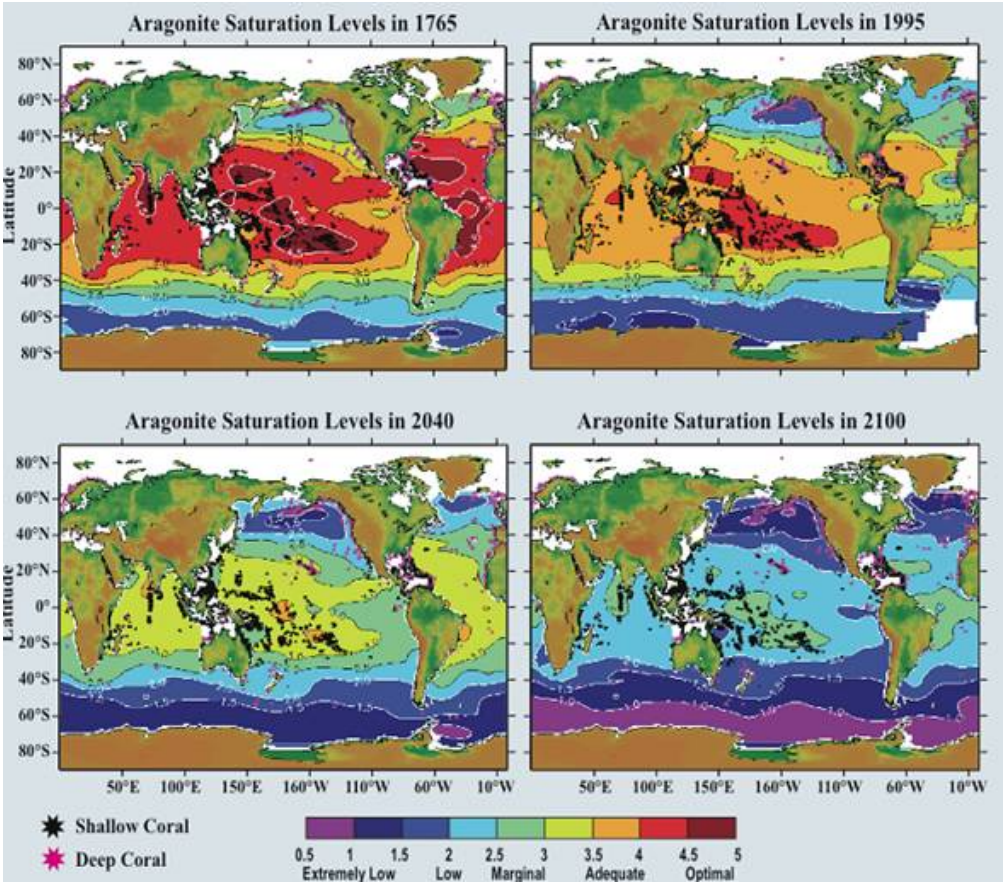

FIGURE 3.1: Estimated aragonite saturation states of the surface ocean for the year 1765, 1995, 2040, and 2100, based on the modeling result of Orr et al. (2005) and a Business-As-Usual CO_2 emissions scenario, Figure extract from Kleypas et al. (2006).

Chapter 4

Ocean acidification and its impact

Although the physical and chemical basis for ocean acidification is well understood, available field data are insufficient in extent, as well as resolution, accuracy for the documentation of acidification rate, and determination of the factors that are responsible for its variability. Dore et al. (2009) presented 20 years of time-series measurements of seawater pH and associated parameters at station ALOHA in the central North Pacific Ocean near Hawaii. They found a significant long-term decreasing trend of –0.0019±0.0002 yr^{-1} in surface pH in agreement with the acidification rate expected from equilibration with the atmosphere. Bates (2007) presented 22 years of continuous CO_2 observations at two sites in the North Atlantic Ocean near Bermuda. The results clearly demonstrate that the ocean has also become more acidic, with a decrease in seawater pH of 0.0012±0.0006 pH units yr^{-1}. Although experiments in the laboratory indicate that acidification reduces the calcification rates of marine calcifying organisms; observation or quantification of biological impact of acidification is not an easy task and has not been done in the field yet. Over the past two decades, there were reports of thinning of shell walls of Arabian Sea foraminifera (Moel et al., 2009), a decrease in the calcium carbonate shell weight of Southern Ocean pteropods (Roberts et al., 2008) and foraminifera (Moy et al., 2009), and corals on the Great Barrier Reef have shown also a decline in the calcification (Cooper et al., 2008). However, more studies are needed to confirm if that is due to the ocean acidification or not. Other studies on marine calcifiers indicate that most but not all of them exhibit reduced calcification

with increased ocean acidification (Fabry et al., 2008). Different marine calcifiers (Figure 4.1) use various mechanisms to control their internal micro-environments where calcification takes place, and also different life stages of marine calcifiers respond differently to increased ocean acidification.

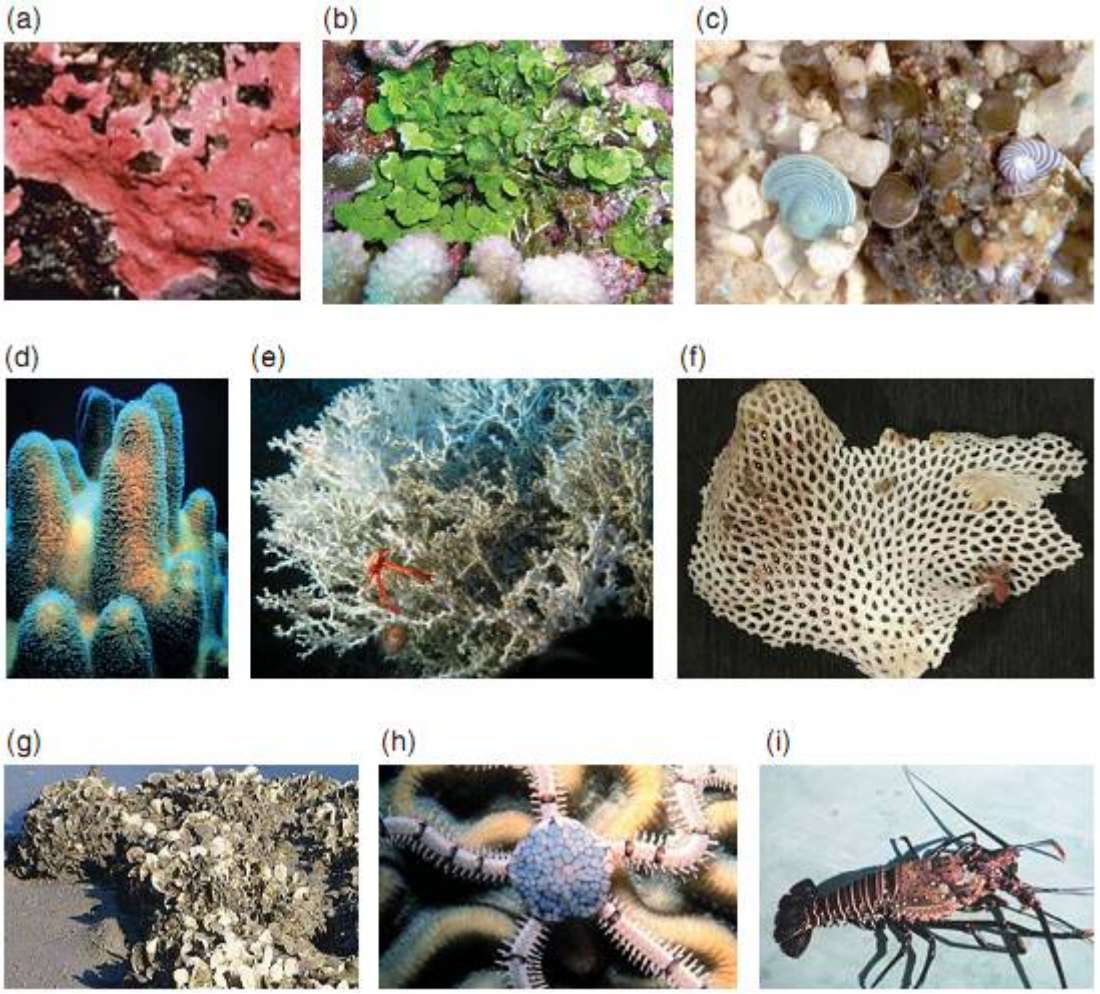

FIGURE 4.1: Representatives of major benthic calcifiers: (a) coralline algae; (b) Hallmeda; (c) benthic foraminifera; (d) reef-building coral; (e) deep-water coral, large red crab is Eumunida picta; urchin below it is Echinus tylodes; (f) bryozoan; (g) mollusk; (h) echinoderm; (i) crustacean. The calcification responses of many of these groups have not been investigated. Figure from Kleypas et al. (2006).

Projected future change of the saturation levels of the aragonite indicates that calcification rates in warm-water corals may decrease by 30% over the next century (Gattuso et al., 1998). Tropical coral reefs are particularly threatened by climate change due to the combined impacts of ocean warming and acidification. Periods

of unusual warmth caused 'coral mass bleaching' killed a large number of corals since 1980s. Corals are large geological structure forms from the skeletons of living organisms and are some of the most biodiverse ecosystems on the planet. Figure 4.2 shows a tropical coral reef and distribution of coral reefs in our area of study; Arabian Sea and the Red Sea. These coral reefs provide food for organisms which live there, protection from flooding caused by storms, income from tourism to hundreds of millions of people, and also acts as nursery and breeding grounds for commercial fishers. Experiments have shown that coral growth rates have decreased in more acidic seawater (Gattuso et al., 1998), at levels of CO_2 and pH predicted for the coming century, although tropical seawater will not become completely corrosive towards corals, reef resilience is likely to become untenable as the delicate balance between accretions and erosion is disturbed, and the same thing will happen to the cold-water or deep-water corals, which are found in the high latitude (Cao and Caldeira, 2008). Figure 4.3 shows pictures of Emiliania huxley taken during a process study investigating the effect of high atmospheric CO_2. The shells appear up normal (distorted) under high pCO_2 (Riebesell et al., 2000). To see the impact on other organisms see Wentworth (2009).

FIGURE 4.2: Left picture shows a tropical coral reef; Right picture indicates by white dots the distribution of these coral reefs in the Arabian Sea and Red Sea. Figure extracted from Bijma et al. (2009).

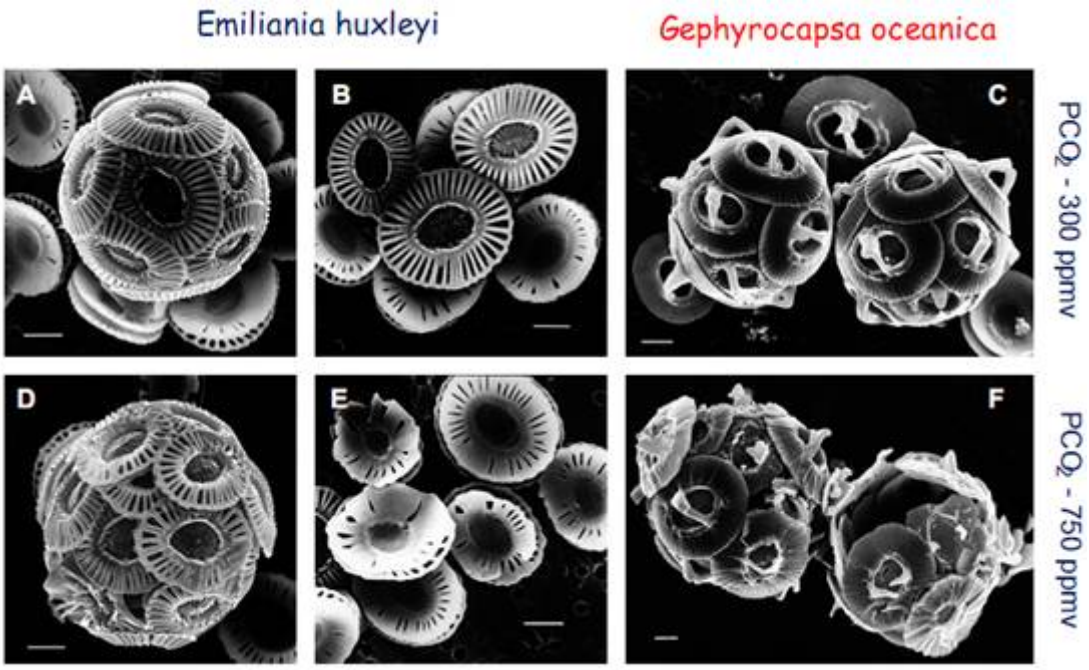

FIGURE 4.3: Pictures of coccolithophores in mesocosm experiments: process studies on how high atmospheric CO_2 affects marine organisms. Figure from Riebesell et al. (2000).

Chapter 5

Description of the area of study

5.1 The Arabian Sea

Arabian Sea (Figure 5.1) is situated in the tropical belt, land-locked in the north (0-25°N and 45-80°E) and forced by seasonally reversing monsoon winds. In addition, it is one of the highest biologically productive regions of the world ocean, due to the summer and winter bloom and also houses a permanent oxygen minimum zone (Kumar et al., 2009b).

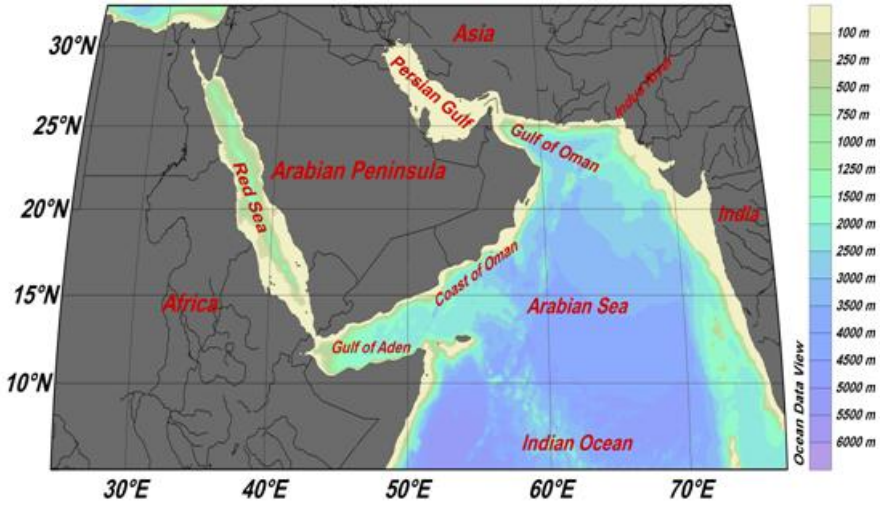

FIGURE 5.1: The location and bathymetry of the Arabian Sea and adjacent areas.

The Arabian Sea has a surface area of about 3,862,000 km^2, maximum width of approximately 2,400 km, and a maximum depth of 4,652 m (Abdel Aleem et al., 2010). The major fresh water input to the Arabian Sea comes from the Indus River (India) and Sindhu River (Pakistan). There are two important branches of the Arabian Sea: the Gulf of Oman to the northwest which connects with the Persian Gulf, and the Gulf of Aden in the southwest which connects with the Red Sea through the strait of Bab Al Mandab. The countries with coastlines towards the Arabian Sea are India, Yemen, Oman, Iran, Pakistan, Sri Lanka, The Maldives, and Somalia.

The continental shelf is narrow along the coast of the Arabian Peninsula and is even narrower along the Somali coast. A few coral reefs are found along the Arabian coast (Figure 4.2). Sediments near Cape al-Hadd (the easternmost headland of the Arabian Peninsula), where upwelling of deep water occurs in summer, consist of fine greenish mud with a high organic content containing hydrogen sulfide. The region, which contains many fish remains, is known as a fish cemetery. Terrigenous (i.e., land–derived) deposits cover the major part of the continental slope to a depth of about 2,700 m. Below this, deposits consist of the calcareous tests (shells) of Globigerina (a genus of protozoans belonging to the Foraminifera order), while basins below 4,000 m are covered by red clay (Abdel Aleem et al., 2010).

The climate and hydrographic conditions of the Arabian Sea is dictated by the monsoonal winds (Figure 5.2). The northeast monsoon blows in December to April, which is the winter time (dry season). The north equatorial current is prominent in this season, the movement of the water is cyclonic, and the mixed layer depth (MLD) extends in the northern Arabian Sea causing weak downwelling near the coast of Oman and upwelling in the central of the Arabian Sea (Figure 5.3). The southwest monsoon blows in June to October (summertime and rainy season), and the region is dominated by the eastward flowing southwest monsoon current. The movement of the water is anticyclonic causing upwelling near the coast of Oman and the MLD extends offshore to the central of the Arabian Sea (Figure 5.3). Between these two seasons are the inter monsoon periods, which describe the transition between the seasons. Because the Equatorial current system in the Indian Ocean are stronger than in the Pacific or Atlantic Oceans during most of the year (Tomczak and Godfrey, 2003), the transition take place faster in

this region. This thesis will focus on the two major monsoon periods, because of a shortage of data for the transitional periods.

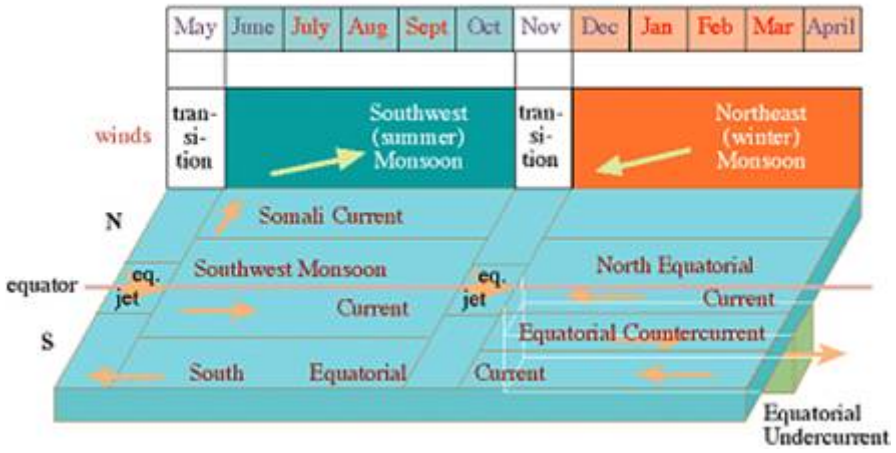

FIGURE 5.2: A summary of the monsoon system in the Indian Ocean, the top part indicates the wind cycle; the lower part shows the major current that develops in response to the wind. Figure from Tomczak and Godfrey (2003).

In the central Arabian Sea surface, minimum temperatures of about 24 to 25°C occur in January and February; while temperatures of about 28°C occur in both June and November (Murray and Johns, 1997). see Figure 5.4.

Sea surface salinity (upper 45 m) is less than 35 during the rainy season when the southwest monsoon blows (June to October), while during the dry season (December to April) when the northeast monsoon blows the salinity is more than 36. Because evaporation exceeds the combined precipitation and river input, the sea exhibits an annual net water loss (Morrison, 1997).

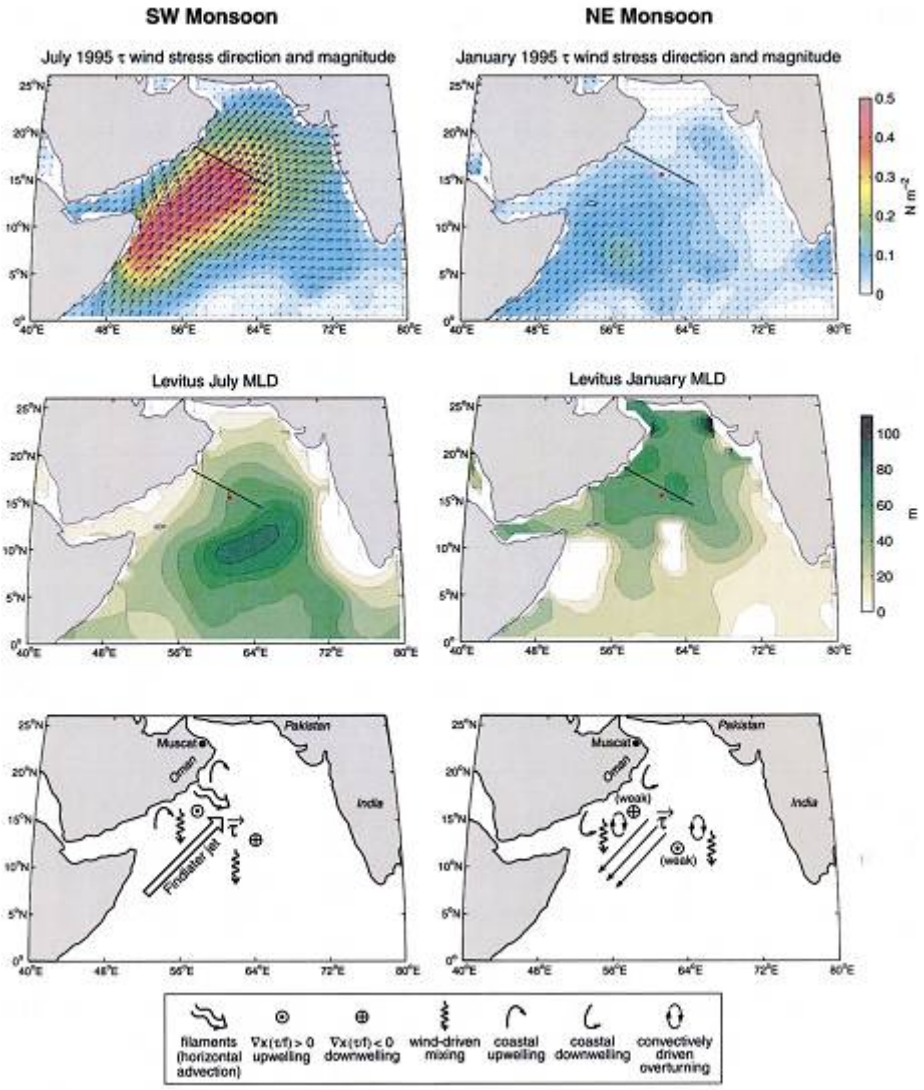

FIGURE 5.3: Southampton Oceanographic Center 1995 windstress (0.02 N m^{2-} contour interval), levitus climatologically mixed-layer depth and schematic representation of the various physical processes that may act during the NE and the SW Monsoon. A black line extending offshore from the Omani Coast marks the US JGOFS Southern line. The large hollow arrow marks the Findlater Jet in the SW Monsoon schematic. Extremely shallow mixed layers in the levitus climatology off the west coast of India during the SW Monsoon and mid-basin during the NE Monsoon are artifacts due to sparse data. Figure from Lee et al. (2000).

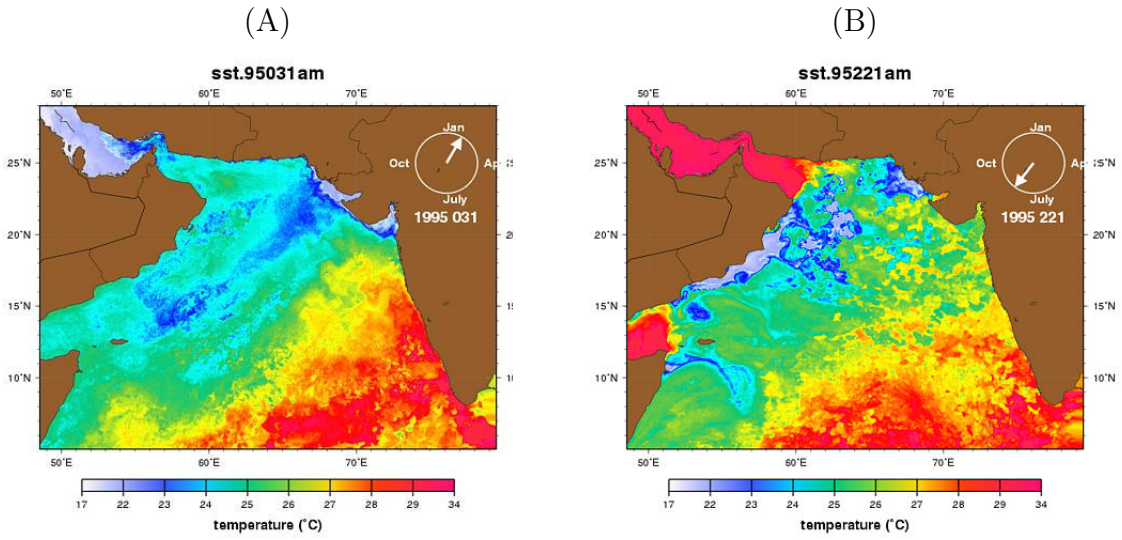

FIGURE 5.4: Sea surface temperature (SST) distribution in the Arabian Sea during (A) winter, and (B) summer season. Figure from http://www.rsmas.miami.edu/personal/eryan/arabian-sst/catalog.html.

5.2 The Red Sea

The Red Sea (Figure 5.5) connects with the Indian Ocean through Bab Al Mandab. It lies between the Arabian Peninsula and Africa, in one of the hottest, driest regions on our planet, and extends from the Strait of Bab Al Mandab at 12.5°N to Ras (cape) Mohammed at the southern part of Sinai Peninsula at 28°N. Table 5.1 presents the Red Sea in numbers. Bab Al Mandab is the only natural gate to the Red Sea from the Indian Ocean, a narrow strait in the south, which connects with the Gulf of Aden. In the north, the sea split into two narrow arms that flank the Sinai Peninsula, the Gulf of Suez, which is connected to the Mediterranean Sea by the Suez Canal, and the Gulf of Aqaba. The Red Sea seems like a deep trench that stretches from north to south for almost the entire sea area. The deepest region lies between 14°N and 28°N, with a maximum depth of 2,920 m. This region is still geological active according to the United Nations Environment program (UNEP, 1997) and has many volcanic vents, emitting hot, salty and material-rich seawater. The Gulf of Suez is shallow and has relatively flat bottom, with depth ranging from 55–73 m. On the other hand, the Gulf of Aqaba is comprised of a deep basin and a narrow shelf with depth 1,000 m, (Figure 5.5).

TABLE 5.1: The Red Sea in numbers, table compiled by Ali (2008).

Area	Fact	Number	Reference
Red Sea	Total surface area	4.5×10^{11} km^2	Patzer (1974)
	Length	1930 km	Patzer (1974)
	Average width	220 km	Patzer (1974)
	Maximum width	2920 km	Morcos (1970)
Gulf of Aqaba	Length	175 km	Cochran (2002)
	Depression depths	1100–1400 m	Edwareds (1987)
Gulf of Suez	Length	300 km	Cochran (2002)
	Range depth	55–73 m	Edwareds (1987)
Bab Al Mandab strait	Average depth	300 m	Maillard and Soliman (1986)
	Narrowest width	18 km	Murray and Johns (1997)
	Sill depth	137 m	Werner and Lange (1975)

There are four water masses in the Red Sea which govern the mass equilibrium of the water, and two of these dominate in the Gulf of Aden, exchanging between the Red Sea and Gulf of Aden passing through Bab Al Mandab throughout the year (Figure 5.6). Red Sea overflow water (RSOW) flows out of the Red Sea

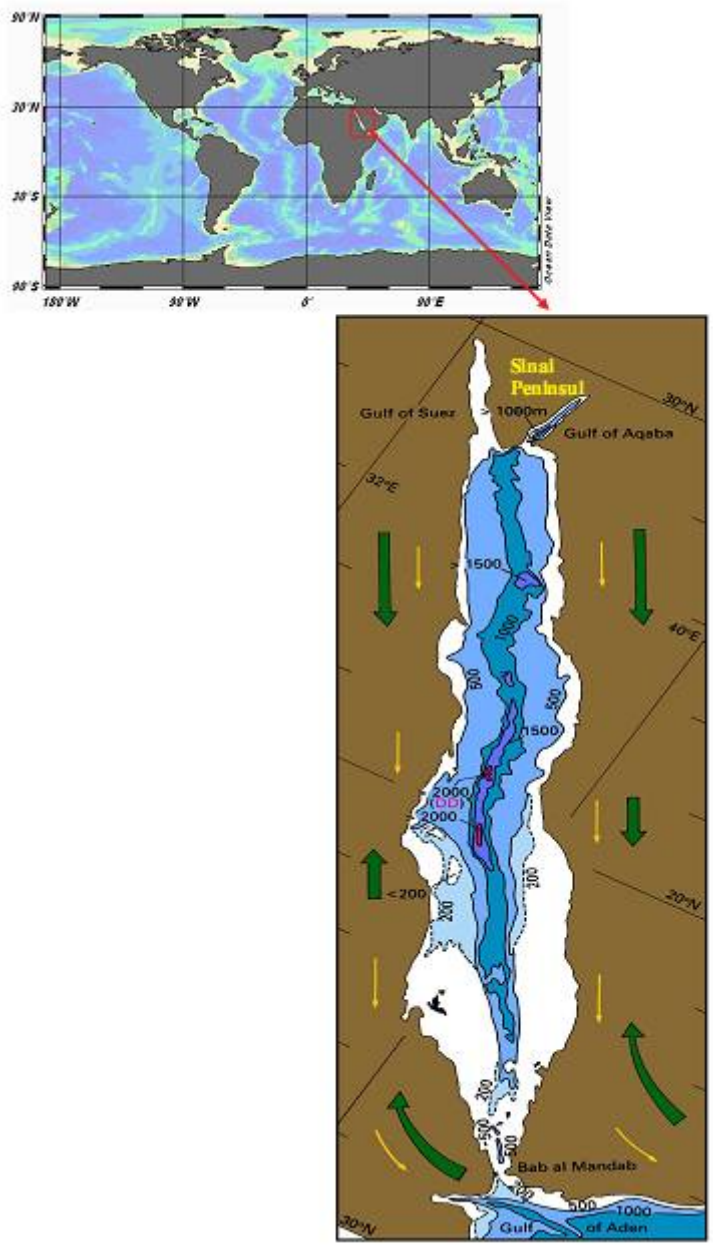

FIGURE 5.5: Maps showing the location and bathymetry of the Red Sea, the thick arrows indicate the prevalent wind directions for summer, and the thin arrows indicate the winter wind direction. Figure from Ali (2008).

through Bab Al Mandab throughout the year. In winter, between November and early June, this flow is balanced by an inflow of Gulf of Aden Surface Water (GASW), and evaporation (0.025 SV) from Red Sea (Souvermezoglou et al., 1989). From June to October (summer season) the southwesterly wind raises an upwelling of Gulf of Aden Intermediate Water (GAIW) (Smeed, 1997) making the water

moving toward the Red Sea. The flux of GAIW to the Red Sea is larger than the outflowing RSOW. In summer the northwesterly winds reaching as far south as Bab Al Mandab, and an outflow of Red Sea Surface Water (RSSW) is induced (Ali, 2008). Also the GASW is forced to reverse in order to balance the inflowing GAIW, and with evaporation from the Red Sea of 0.035 SV the volume budget is balanced (Sofianos et al., 2002). The mass balances are shown in Figure 5.6, and for more information see Ali (2008) and references therein.

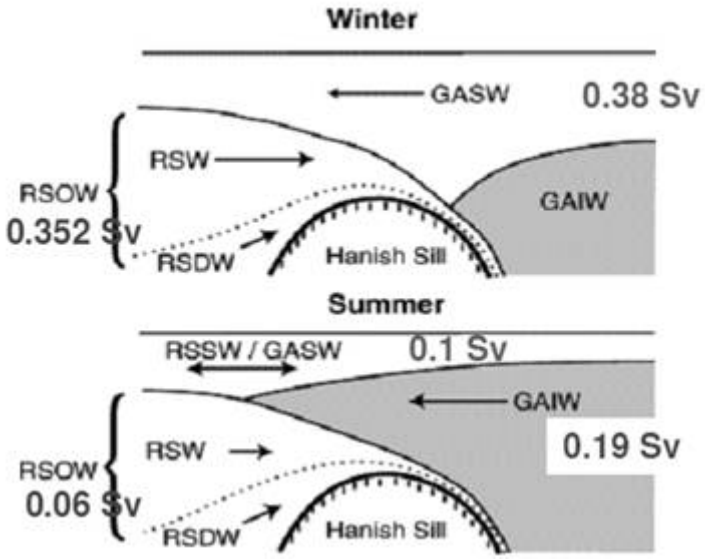

FIGURE 5.6: Schematic of the winter and summer water mass exchange. Figure from Smeed (1997).

The SST vary between 24 and 30°C with the highest values in the central Red Sea, due to the weak wind most of the year (Sofianos and Johns, 2003). The visibility remain good to around 200 m. Below 300 m the temperature is about 21.5°C continuing to the bottom (Figure 5.7), thus, the Red Sea embody the warmest deep water in the world.

SSS increases from ∼36 in the southern part of the Red Sea due to the exchange of Gulf of Aden water mass, to >41 in the northern part, and the average salinity is about 40 (Figure 5.8). The Red Sea is higher in salinity compared to the world average, this is due to several factors: High rate of evaporation and little precipitation, lack of significant rivers draining into the sea; and limited connection with the lower salinity Indian Ocean water.

The northern part of the Red Sea is dominated by north-west winds, with speeds between 1.9 and 3.3 ms^{-1}. The rest of the Red Sea and the Gulf of Aden are influenced by regular and seasonally reversible monsoon winds similar to the situation in the Arabian Sea. The wind regime is characterized by both seasonal and regional variations in speed and direction with the average speed generally increasing northward (Figure 5.9). Wind is also the driving force in the Red Sea for transporting material either as suspension or as bedload. Wind induced currents play an important role in the Red Sea in initiating the process of resuspension of bottom sediments and transfer of materials from sites of dumping to sites of burial in quiescent environment of deposition (Morcos, 1970). Measurement of wind generated current is therefore important in order to determine the sediment dispersal pattern and its role in the erosion and accretion of the coastal rock exposure and the submerged coral beds.

Temporal and spatial currents variability is as low as 0.5 m s^{-1}, and is dominated mostly by wind. Northwest winds drive the surface water south for about four months at a velocity of 15-20 cm s^{-1} in summer, whereas in winter the flow is reversed resulting in inflow of water from the Gulf of Aden into the Red Sea. The net value of the latter predominates, resulting in an overall drift to the northern end of the Red Sea. In general the velocity of the tidal current is between 50-60 cm s^{-1} with a maximum of 1 m s^{-1}, at the mouth of the Al-Kharrar Lagoon north of Jeddah in the east coast of the Red Sea. However, the range of north-northeast current along the Saudi coast is 8-29 cm s^{-1}.

The tide ranges between 0.6 m in the north, near the mouth of the Gulf of Suez and 0.9 m in the south near the Gulf of Aden, and it fluctuates between 0.20 m and 0.30 m away from the nodal point (PERSGA, 1998).

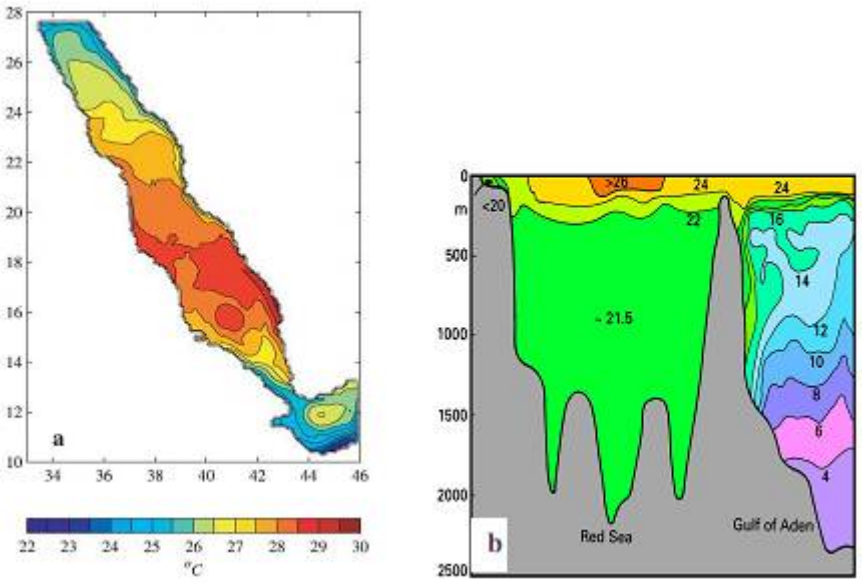

FIGURE 5.7: The temperature distribution in the Red Sea (a) surface and (b) water column. Figure from Sofianos and Johns (2003); Tomczak and Godfrey (2001).

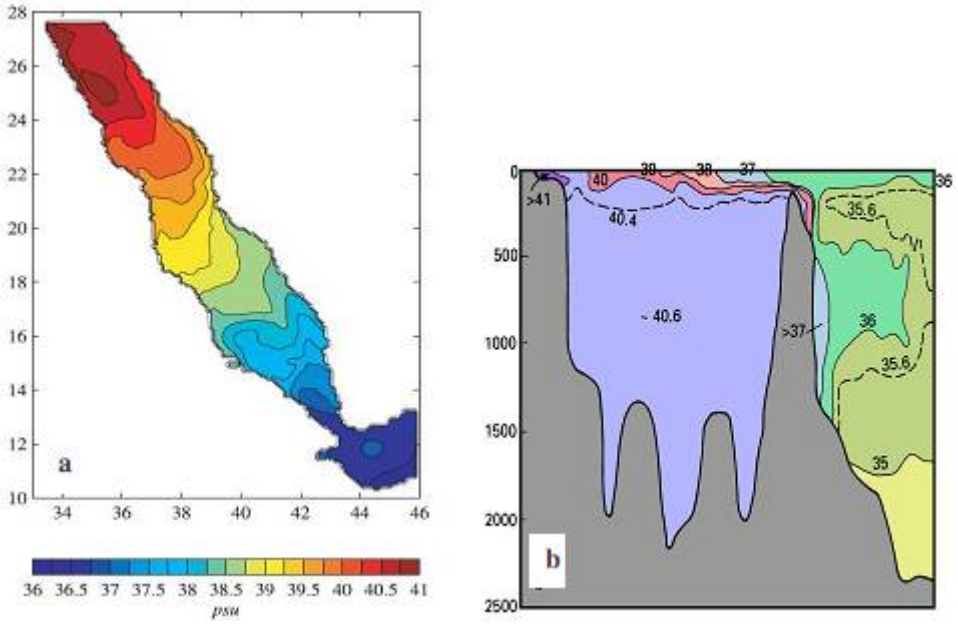

FIGURE 5.8: The salinity distribution in the Red Sea (a) surface and (b) water column. Figure from Sofianos and Johns (2003); Tomczak and Godfrey (2001).

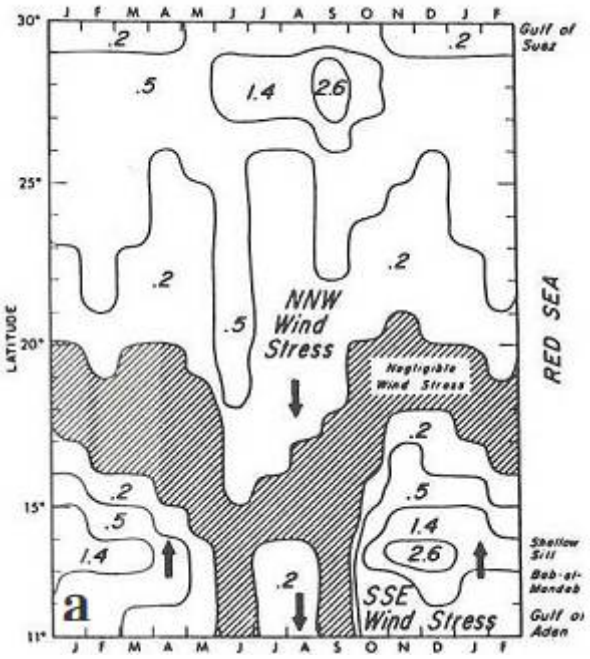

FIGURE 5.9: Monthly mean wind stress at the Red Sea surface (dynes per square centimeter). Figure from Patzer (1974).

Chapter 6

Data and method

Three datasets were used in this study. These are summarized in Table 6.1 and a brief description of each of the datasets is given below.

GEOSECS Data 1977: GEOSECS is an abbreviation for Geochemical Ocean Section Study which was a global survey of the three-dimensional distribution of chemical, isotopic, and radiochemical tracers in the oceans. As part of the Indian Ocean survey on December 1977 to March 1978 samples were collected from the Red Sea, see Figure 6.1. The data are available on `http://iridl.ldeo.columbia.edu/SOURCES/GEOSECS/`, and the variables which were determined are shown in Table 6.1. According to Bradshaw et al. (1981) error of C_T was +12 μmol kg^{-1}, while the A_T data didn't have any offset.

Merou Data 1982: The Merou cruise by R/V MARION DUFRESNE took place during 16^{th} June to 4^{th} July 1982 (1982 A, or Merou A), and from 25^{th} September to 9^{th} October 1982 (1982 B, or Merou B). During each part of the cruise, a longitudinal section in the Red Sea was carried on, as well as five cross sections in the strait of Bab Al Mandab, and several sections in the Gulf of Aden (Papaud and Poisson, 1986). Figure 6.1. shows the stations which were used in our study. At each station a number of samples were collected, see Table 6.1. The accuracy for temperature, salinity, C_T and A_T were 0.005°C, 0.02, 0.1% and 0.3%, respectively.

Arabian Sea data 1995: This data is from the US JGOFS (The United State Joint Global Ocean Flux Study), which was a national component of international JGOFS and an integral part of global climate change research (http://usjgofs.whoi.edu). The Arabian Sea process study field work took place onboard the R/V Thomas G. Thompson, starting in October 1994 and ending in January 1996. For our study we selected five cruises which show the monsoonal variation clearly (winter and summer), Table 6.1 and Figure 6.1. The cruises took place between the 8^{th} of January until 26^{th} of December 1995, and by this covering an annual cycle. The precision of the A_T and C_T data were ± 3.2 and ± 2.7 μmol kg^{-1}, respectively (Millero et al., 1998).

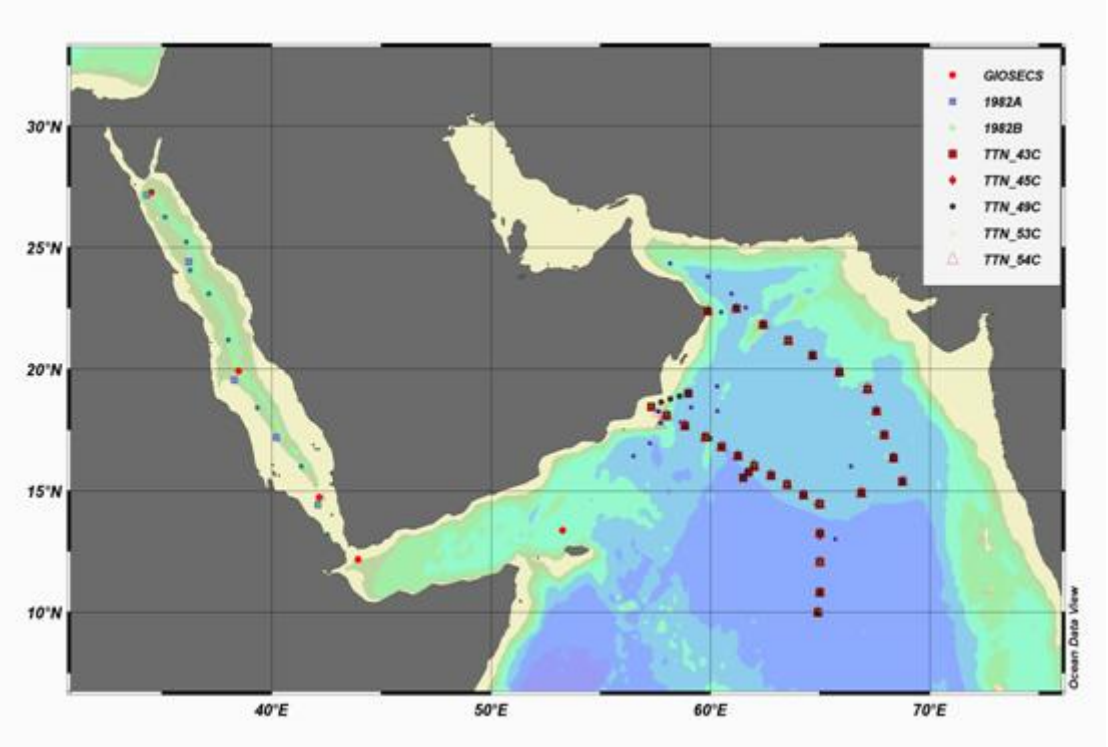

FIGURE 6.1: Sample stations in the Arabian Sea and Red Sea, indicate in the legend by TTN for Arabian Sea and GEOSECS, 1982A, and 1982B for Red Sea.

All the data were merged into one file and the software Ocean Data View (ODV) was used for the interactive exploration and graphical display of the data. The program is available from: http//odv.awi.de.

For the Merou B cruise no CTD salinity was available so bottle salinity was used. pH_T was calculated using the program CO2SYS (Lewis and Wallace, 1998) with the constants of Mehrbach et al. (1973) and Kso_4 (the dissociation constant for the reaction in Eq. 6.1) (Dickson, 1990);

$$HSO_4^- \longrightarrow H^+ + SO_4^{2-} \tag{6.1}$$

$$Kso_4 = \left[H^+\right] \frac{\left[SO_4^{2-}\right]}{\left[HSO_4^-\right]} \tag{6.2}$$

This program also provides information about the carbonate ion concentration (CO_3^{2-}) and the degree of saturation for aragonite (Ω Ar) and calcite (Ω Ca). The original DOS version of CO2SYS was converted to Matlab by Denis Pierrot, University of Miami, and it's available on CDIAC (Carbon Dioxide Information Analysis Center) (`http://cdiac.ornl.gov/oceans/CO2rprt.html`).

TABLE 6.1: Summary of the datasets used in this thesis

Data set	Month & year	No. of stations	Location	Parameters										
				T	S	O_2	PO_4	NO_2	NO_3	SIO_4	AOU	A_T	C_T	pH
GEOSECS	Dec 1977	5	R.S, G.A	+	+	+	+	−	+	+	+	+	+	−
MEROU-A	Jun 1982	5	R.S	+	+	+	+	+	+	+	−	+	+	−
MEROU-B	Oct 1982	10	R.S	+	+	+	+	+	+	+	−	+	+	−
US.JGOFS TTN-043	Jan 1995	30	A.S	+	+	+	+	+	+	+	−	+	+	−
US.JGOFS TTN-045	Mar 1995	30	A.S	+	+	−	−	−	−	−	−	+	+	+
US.JGOFS TTN-049	July 1995	34	A.S	+	+	+	+	+	+	+	−	+	+	−
US.JGOFS TTN-053	Nov 1995	26	A.S	+	+	−	−	−	−	−	−	+	+	−
US.JGOFS TTN-054	Dec 1995	29	A.S	+	+	−	−	−	−	−	−	+	+	+

(+) means parameter determined, and (−) means parameter not determined.
R.S means Red Sea, G.A means Gulf of Aden, and A.S means Arabian Sea.

Chapter 7

Result and discussion

7.1 Surface distribution

During winter, the Sea Surface Temperature (SST) in the northern region of the Arabian Sea is 25°C and increases to 27–28°C as we move to the south (Figure 7.1A). This is connected to the relatively cool, dry NE wind, coming from the land and hiting the surface Arabian Sea which it cool, so the north region will be a bit colder than the southern region. This wind induces week downwelling near the Omani coast, and weak upwelling in the central Arabian Sea due to the overturning of the water there (Figure 5.3). The northern Red Sea has lower SST (about 23°C) than the south which has temperatures of about 26.7°C. The highest SST exceeds 27°C and is observed in the central parts of the Red Sea, and that is related to the very week wind speeds which dominate this region most of the year (Sofianos and Johns, 2003). The northern Red Sea (19°N to 30°N) is influenced by the eastern Mediterranean weather system (cool and rainy in winter) and the wind blows from the northwest all year around (Ali, 2008). The south region is directly influenced by the Indian monsoonal seasons.

The winter distribution of Sea Surface Salinity (SSS) is shown in Figure 7.1B. In the northern Red Sea SSS exceed 40 and decrease to the south to 37 in the strait of Bab Al Mandab. The low values in the south are due to less saline water entering the Red Sea from the Gulf of Aden. Since evaporation exceeds precipitation in this

region, the water become more salty as it flows northwards. Eventually it becomes so dense that it sinks and turns back towards the Gulf of Aden as intermediate Red Sea water out flow. In Arabian Sea the saline water appears in the north east region with a value of 36.5, which is connected to the advection of the saline surface water of the Persian Gulf through the Gulf of Oman (Tomczak and Godfrey, 2003). The south region appears to be fresher due to the north equatorial current which is carrying low salinity surface water westward. Also in the west of the Arabian Sea the water appears with low salinity and is most likely due to the mixtures between the southern hemisphere waters (low salinity) which enters this region during the intermonsoon, and the higher salinity waters which is normally found here (Morrison, 1997).

In contrast, during the summer season when the southwest monsoon (SW) dominates all over the Arabian Sea and southern Red Sea, the hydrology is different, (Figure 5.3). The SW monsoon is warm with high wind speeds, moist air prevails, and upwelling occurs near the Omani coast. That results in SST of about 23°C in the Omani coast and increasing SST offshore to 27°C (Figure 7.2A). Costal upwelling also affects the SSS as fresher water appears near the Omani coast with salinities about 35.9. SSS increases offshore to 36.7 (Figure 7.2B). In the Red Sea northwesterly wind (dry and cool) dominates during summer and the SST is 3°C higher compared to the winter season (about 27°C) and increase to the south to 31°C. The SSS distribution shows the fresh water in the south where Gulf of Aden water with a salinity of 36.6 enters into the Red Sea. The SSS increases northwards to >40 as seen during winter season (Ali, 2008).

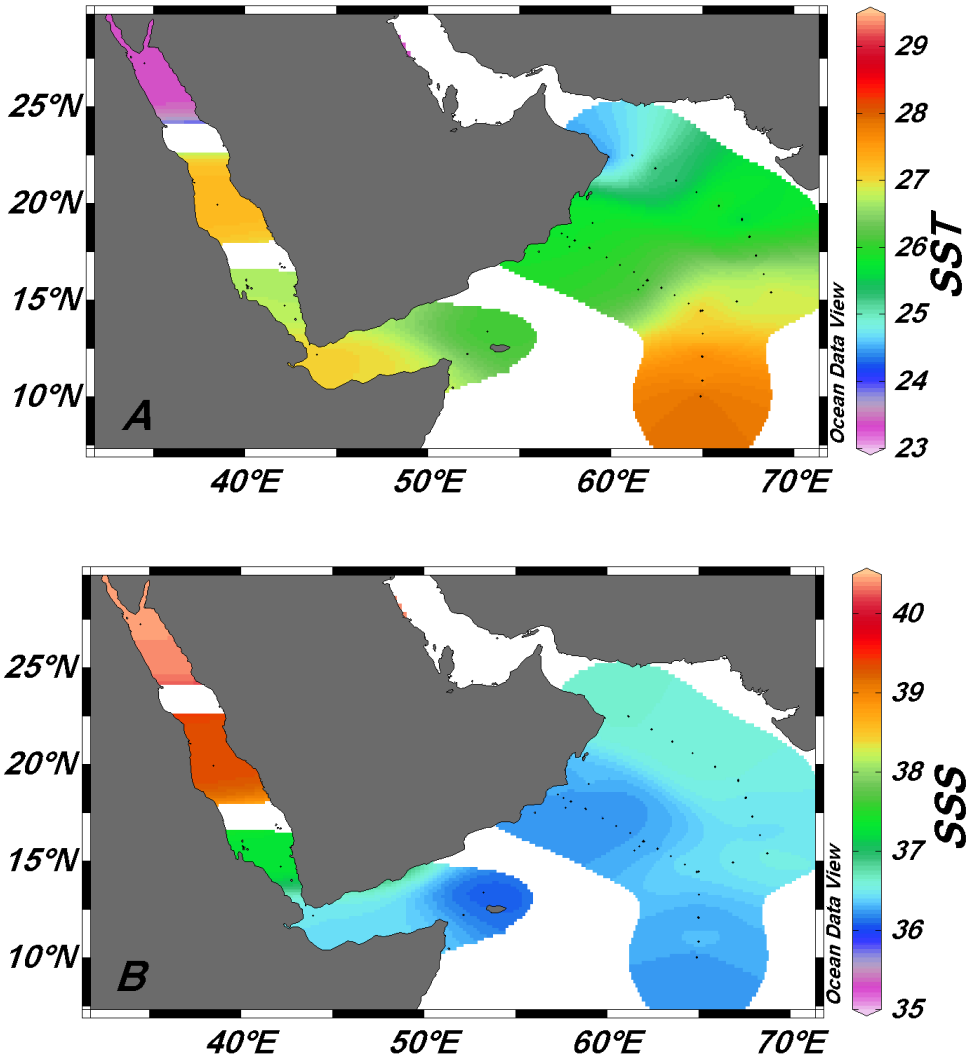

FIGURE 7.1: Surface winter distribution of (A) temperature (SST) by °C and (B) salinity (SSS) in the upper 50 m of the Arabian Sea and the Red Sea.

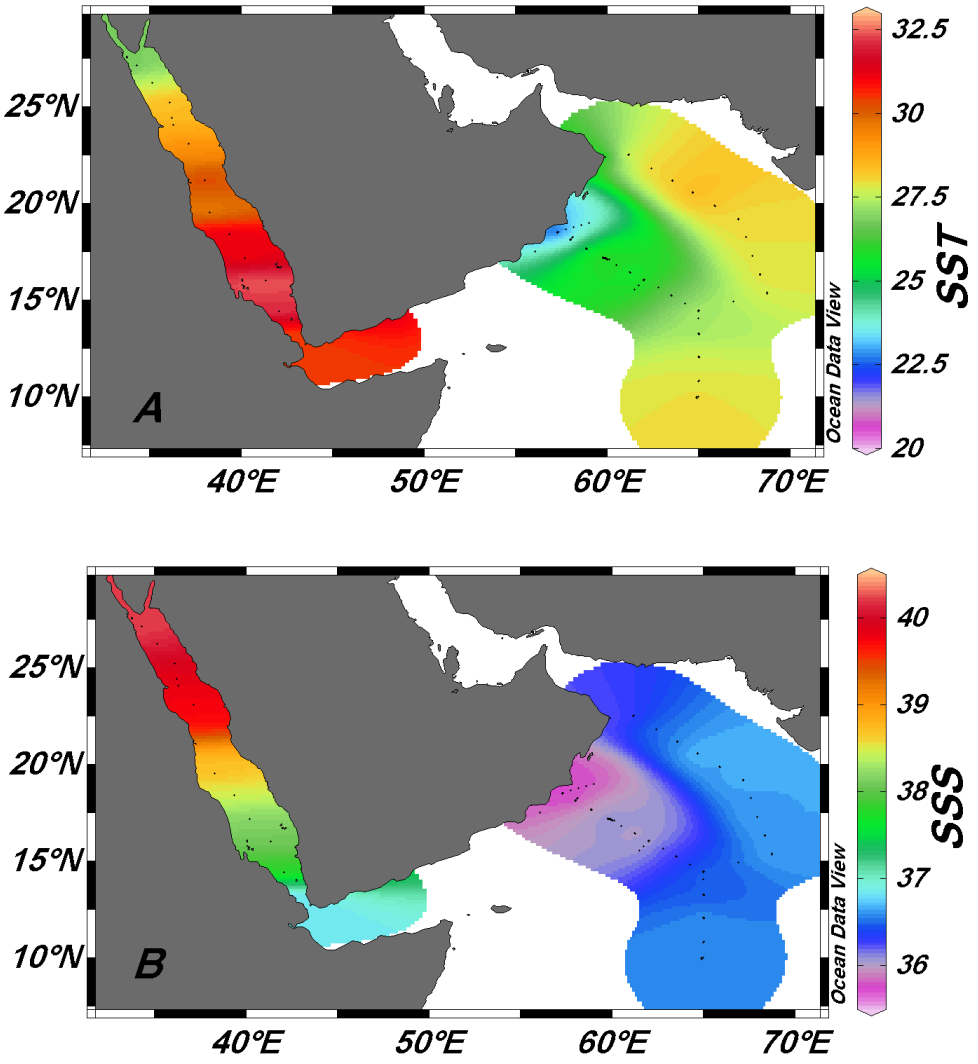

FIGURE 7.2: Surface summer distribution of (A) SST by °C and (B) SSS in the upper 50 m of the Arabian Sea and the Red Sea.

The distributions of C_T in the surface water during the winter season are shown in Figure 7.3A. A high concentration in C_T of about 2070 μmol kg^{-1} is observed in the north of the Red Sea decreasing to the south. In the Arabian Sea relatively high C_T concentrations were found in the north and northeast (2050 μmol kg^{-1}) and low concentrations are found in the west and south. The C_T distribution during winter of both regions is semi related to the temperature and the salinity (Figure 7.1) with contribution of eddies activity in the Arabian Sea. The eddies dominate the area and account for 85–95% of the total variance in surface currents (Flagg and Kim, 1998). The decreasing of the C_T southward is due to the increasing temperature southward, the low temperature in the northern region in both seas increase the solubility of the CO_2 and leads to high C_T.

During summer (Figure 7.3B), the concentrations of C_T approaches 2144 μmol kg^{-1} in the Omani coast in the Arabian Sea, and decrease offshore to 2020 μmol kg^{-1}. The coastal values are due to the upwelling which brings deep water rich of dissolved inorganic carbon to the surface, this carbon was generated during the remineralization processes in the intermediate water. The Red Sea summer concentrations of C_T were found approaching 2057 μmol kg^{-1} in the northern region, and decreasing to the south. Summer C_T in the Red Sea is less thanthat of the winter season (Figure 7.3) primarily due to the inflow of the Gulf of Aden surface water rich of CO_2 in the winter season.

From the C_T figures, it can be observed that the major processes controlling this distribution were temperature, biological productivity, and upwelling. To see the effect of the biology in the Arabian Sea and Red Sea, C_T was plotted against nitrate (NO_3) in Figure 7.4A. The good correlation between the two variables shows that upwelling and subsequent primary production have huge impact in controlling the surface concentration of C_T. For The Red Sea the correlation is weaker and other processes may be more influential than organic matter production/remineralization in controlling C_T. This is in agreement with Ali (2008) who suggested that about 25% of the surface C_T variation in the Red Sea was due to the air-sea gas exchange. The latter process also affects surface C_T in the Arabian Sea and this gives rise to the relatively strong inverse correlation with SST shown in Figure 7.4B.

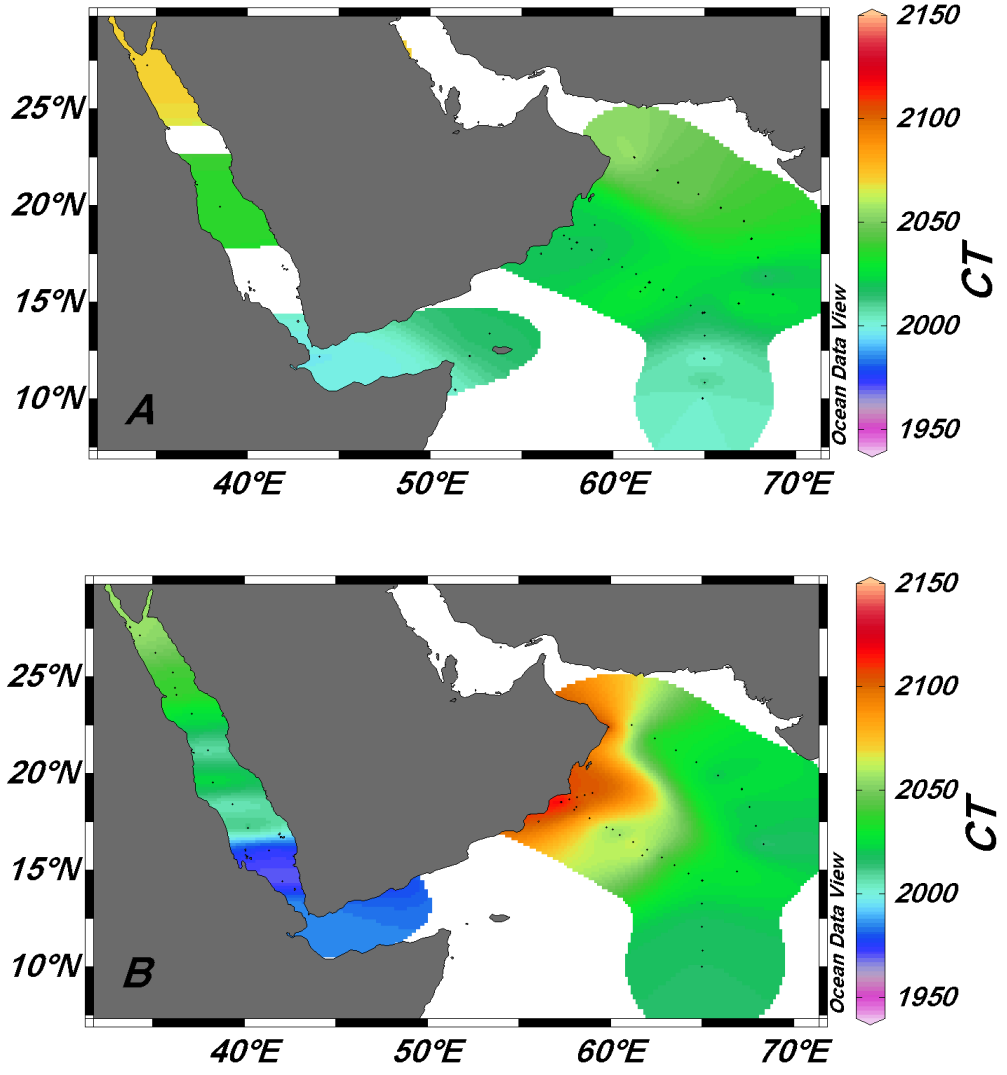

FIGURE 7.3: Distribution of C_T [μmol kg^{-1}] in the upper 50 m of the Arabian Sea and the Red Sea during (A) winter and (B) summer seasons.

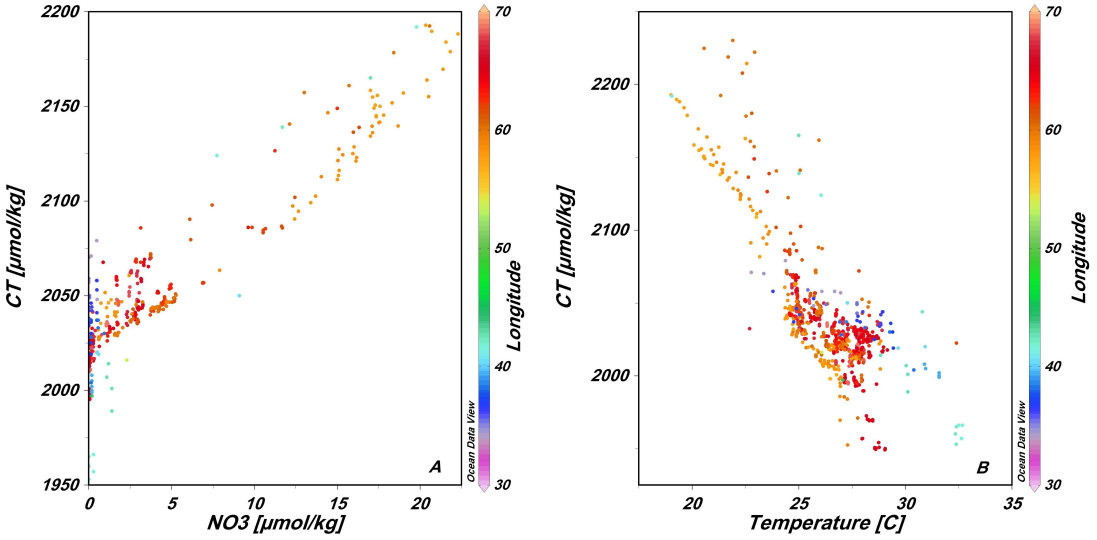

FIGURE 7.4: The relation between (A) C_T and NO_3, and (B) C_T and temperature in the upper 50 m of the Arabian Sea (55 °E–70°E) and Red Sea (30°E–45 °E) throughout the year.Longitude is shown as color in Z axis to separate the two regions.

The distributions of A_T in the surface water during the winter and summer seasons are shown in Figure 7.5. A high A_T concentration of about 2470 μmol kg^{-1} is observed in the north of the Red Sea during both seasons and the concentration decreases towards the south where less saline water enters from the Gulf of Aden. Also evaporation results in higher A_T as the water flows northwards. In the Arabian Sea relatively high A_T concentrations (about2400 μmol kg^{-1}) were found in the north and northeast, and low concentrations are found in the west and south (Figure 7.5A) in winter season. During the summer season low A_T values ($\approx$ 2325 μmol kg^{-1}) were found near the coast of Oman (Figure 7.5B) and this increased offshore due to the upwelling which brings deep low salinity, high NO_3, and low alkalinity water to the surface.

For both seas, the surface distribution of A_T shows a good relationship with the salinity (Figure 7.6). The correlation indicates that surface A_T is mainly influenced by salinity variations in both regions. If one extrapolates the line defined by the Arabian Sea datapoints, all the Red Sea data points fall under this line. This indicates that there is a loss of A_T in the Red Sea due to CO_3^{2-} loss through calcification and probably also sedimentation (Elageed, 2010).

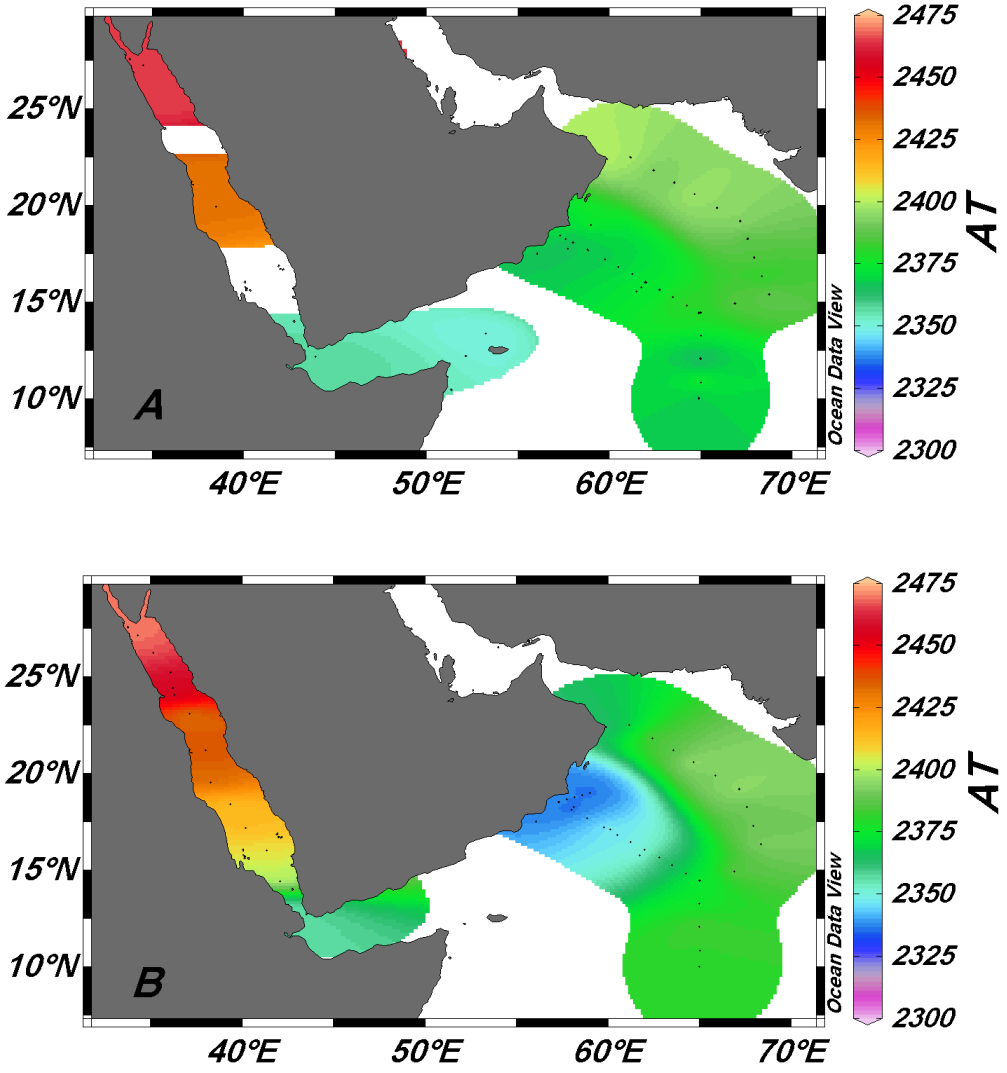

FIGURE 7.5: Distributions of A_T [μmol kg^{-1}] during (A) winter and (B) summer seasons in the upper 50 m of the Arabian Sea and Red Sea.

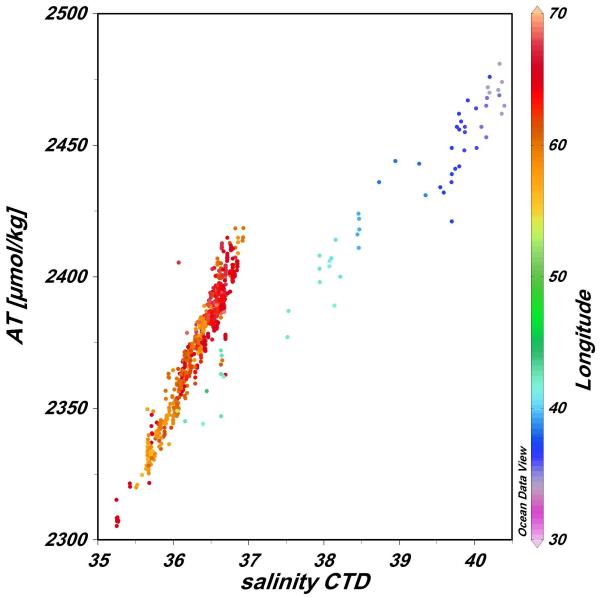

FIGURE 7.6: Surface alkalinity as a function of salinity in the Arabian Sea (55°E–70°E) and Red Sea (30°E–45°E) in the upper 50 m throughout the year. Longitude is shown as color in Z axis to separate the two regions

The surface pH distribution during winter season shows high values in the north of the Red Sea (about 8.12) and decreasing values southwards (Figure 7.7A). Since both A_T and C_T increase northwards by about 100 μmol kg^{-1} during winter (Figures 7.4–7.6), the northward increase in pH must be associated with low temperatures in the north. This hypothesis draws further support from the fact that during summer (Figure 7.7B), minimum pH values are found in the central parts of the Red Sea which also show maximum SST values due to the wind convergence.

The Arabian Sea during winter season shows pH variation of 8.09 to 8.05 (Figure 7.7A). There are relatively high pH values along the coast of Oman and that is connected to the high biological productivity near the coast supported from the nutrients which are brought up by mixing driven by winter cooling and wind, as evidenced by the correlation between the nutrients and pH (Figure 7.8). Another factor which may relatively influence the pH in this season is temperature i.e. pH decreases southward and temperature increases southward. In summer season, the most remarkable feature in the Arabian Sea is the low pH values at the Omani coast (7.93) and the increasing pH offshore to 8.06. This is due to upwelling, which brings cold intermediate water rich in CO_2 and nutrients to the surface. As biological productivity utilizes carbon and nutrients, the pH increases away from

the Omani coast. This is depicted in Figure 7.8 which shows a good correlation of the nutrients with pH and in Figure 7.9 which shows the correlation of the temperature with pH. Those figures shows that the biological production and the temperature sustained by the upwelling were the common processes which affect the changes on pH of the Arabian Sea during the year, while the pH in the Red Sea was largely affected by the temperature.

It is interesting to note that during summer the Omani coast pH is about 0.14 units lower than the average pH in the Arabian Sea. This difference is much greater than the entire pH reduction due to anthropogenic carbon since the onset of the industrial revolution, 0.1 units (Raven et al., 2005). This observation makes the Arabian Sea particularly suitable for ocean acidification studies.

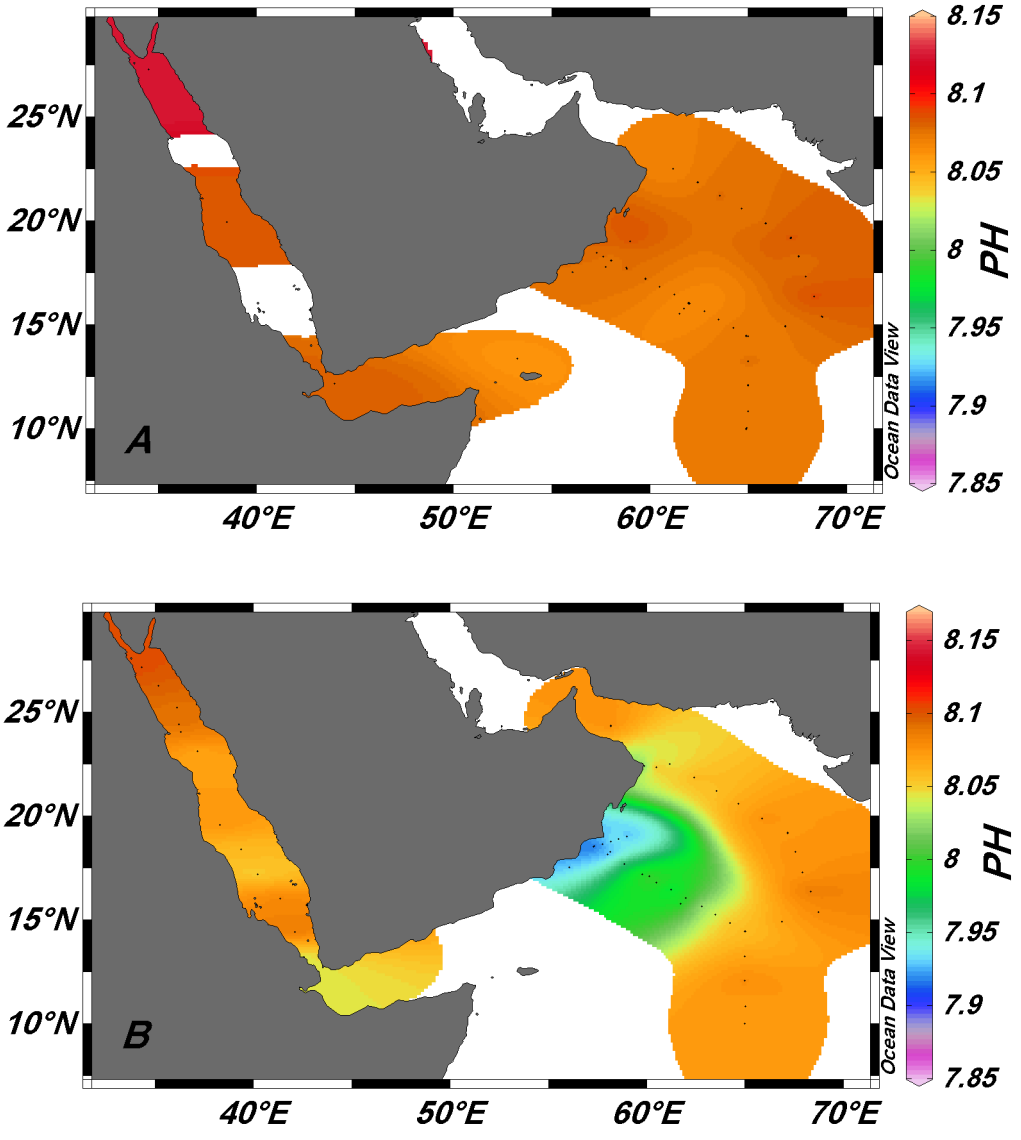

FIGURE 7.7: Surface pH (upper 50 m) distribution of the Arabian Sea and the Red Sea during (A) winter and (B) summer.

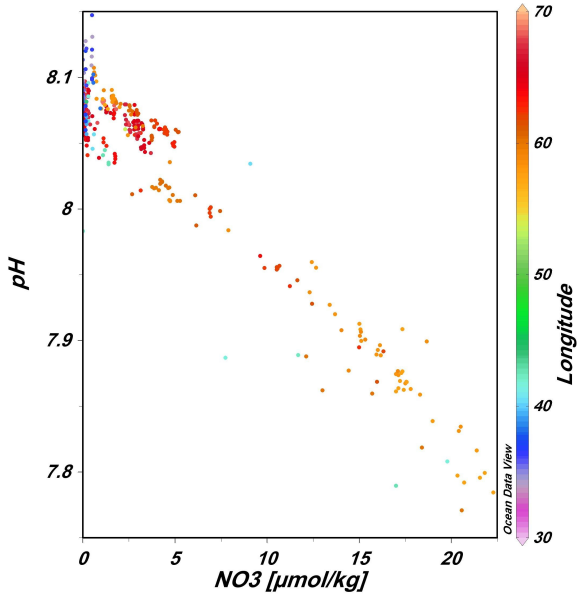

FIGURE 7.8: pH as a function of NO_3 in the upper 50 m of the Arabian Sea (55°E–70°E) and the Red Sea (30°E–45°E) during the whole year. Longitude is shown as color in Z axis to separate the two regions.

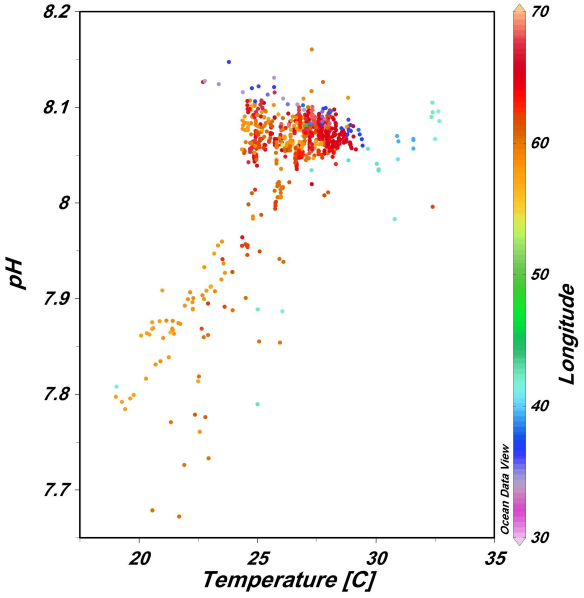

FIGURE 7.9: pH as a function of temperature in upper 50 m of the Arabian Sea (55°E–70°E) and the Red Sea (30°E–45°E) during the whole year. Longitude is shown as color in Z axis to separate the two regions.

The surface of the Arabian Sea is supersaturated with respect of aragonite and calcite during winter and summer seasons, as shown in Figures 7.10 and 7.11. During winter the saturation degree (Ω) values are high in the coast of Oman and

in the south (4.09 and 6.15 for aragonite and calcite, respectively), and slightly lower in the Omani Gulf and west of the Arabian Sea (Figures 7.10A and 7.11A). In contrast, during summer season the coast of Oman shows the lowest Ω values (2.13 and 3.28 for aragonite and calcite, respectively), and the Ω values increase offshore (Figures 7.10B and 7.11B). The biological production of hard parts, such as shells and skeleton, is the major process affecting the degree of saturation, and in addition also the air-sea CO_2 exchange, physical mixing, fresh water input and changes in temperature affect the degree of the saturation. Cold and fresh water promotes lower $CaCO_3$ degree of saturation (Chierici and Fransson, 2009), which might explain what is happening in the north and the west part of the Arabian Sea in winter season (Figures 7.10A and 7.11A) and at the coast of Oman in the summer season, where the upwelling brings cold and fresh intermediate water to the surface.

The Red Sea Ω values during winter were 4.0 to 4.24 for aragonite and 6.0 to 6.36 for calcite, with highest values in the central parts (Figures 7.10A and 7.11A), possible due to the high temperatures in the centre of the Red Sea. During summer the saturation degree for aragonite were 4.41 to 4.96 and for calcite 6.6 to 7.3 (Figures 7.10B and 7.11B) with the highest values in south and decreasing values towards the north. This might connected to the high temperature in the south leading to a decrease in the calcium carbonate solubility.

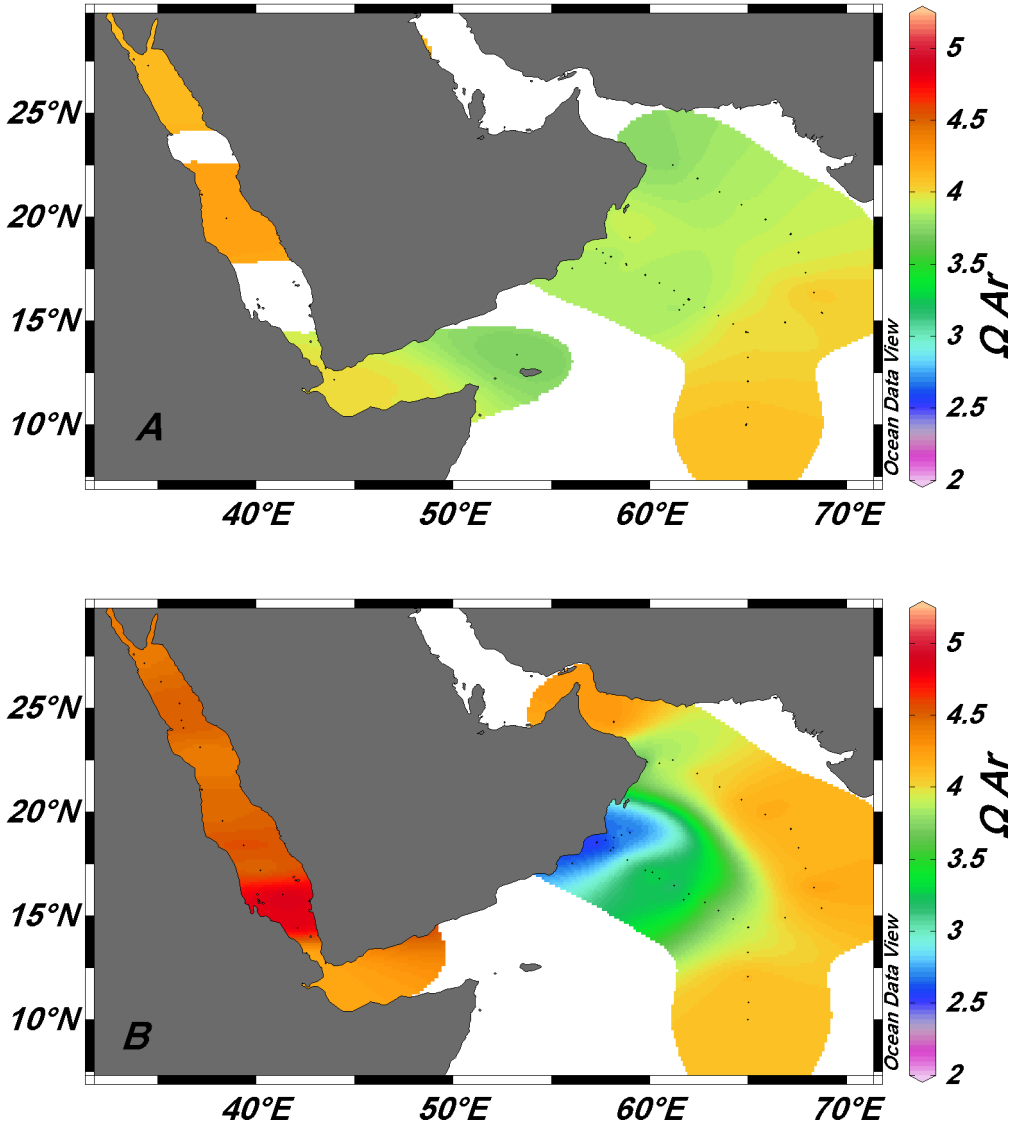

FIGURE 7.10: The surface distribution of the degree of saturation of the aragonite (ΩAr) during (A) winter and (B) summer in the upper 50 m of the Arabian Sea and Red Sea.

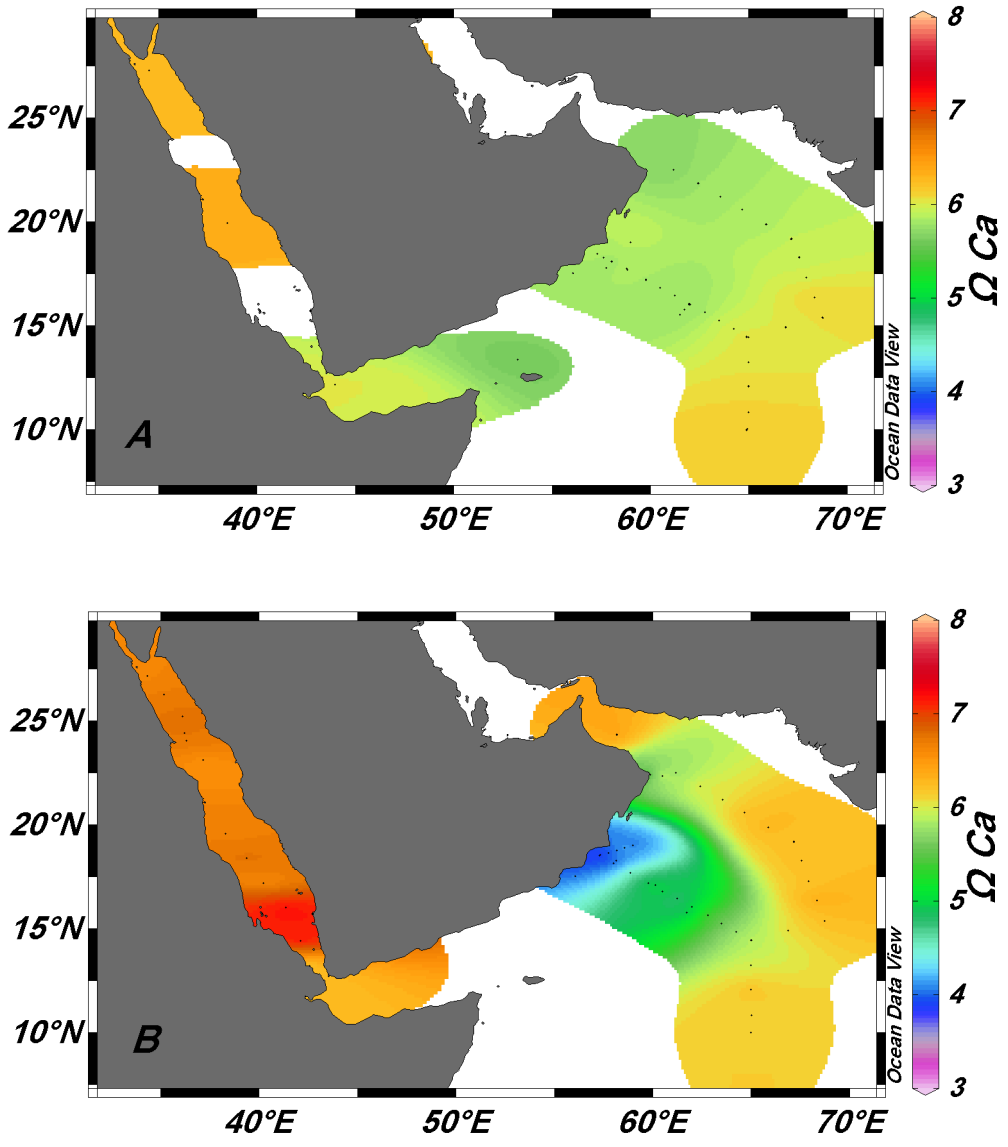

FIGURE 7.11: The surface distribution of the degree of saturation of the calcite (ΩCa) during (A) winter and (B) summer in the upper 50 m of the Arabian Sea and Red Sea.

7.2 Vertical distribution

To examine the vertical distribution, all the data are plotted together ignoring the monsoonal variation, since this will not affect the vertical water masses. In Figure 7.12 pH, temperature, pH at constant temperature, CO_3^{2-} concentration, alkalinity, and degree of saturations of aragonite and calcite are plotted against depth for the Arabian Sea and Red Sea. Both pH and CO_3^{2-} concentration (Figures 7.12A and 7.12D) are high in the surface layers due to the photosynthesis, which consume CO_2, and the values decrease rapidly in subsurface waters due to the release of CO_2 primarily from respiration processes. Between about 100 and 1500 m in the Arabian Sea, the increase in pH due to decreasing temperature (Figures 7.12A and 7.12C) is almost balanced by the decrease in pH resulting from the fact that C_T increases more than A_T (Figures 7.12E and 7.12F) due to the oxidation of the organic matter. This produces somewhat stable pH until 1500 m (Figure 7.12A). Below this depth and until about 2500 m pH values increase due to decreasing temperature. From 3000 m the pH is stable.

From Figures 7.12G and H it is seen that the Arabian Sea becomes undersaturated ($\Omega<1$) with respect to aragonite between 400 to 600 m and with respect to calcite between 3000 to 3500 m. In contrast, the Red Sea is supersaturated all over the water column. Thus, loss of carbonate due to sedimentation is highly possible in the Red Sea. Further, the depth of undersaturation with respect to aragonite is much shallower in the Arabian Sea compared with the others regions in the ocean. This is due to the upwelling of old waters which have acquired more CO_2 from the cumulative effects of respiration while they travel along the transport pathway of the deeper water masses.

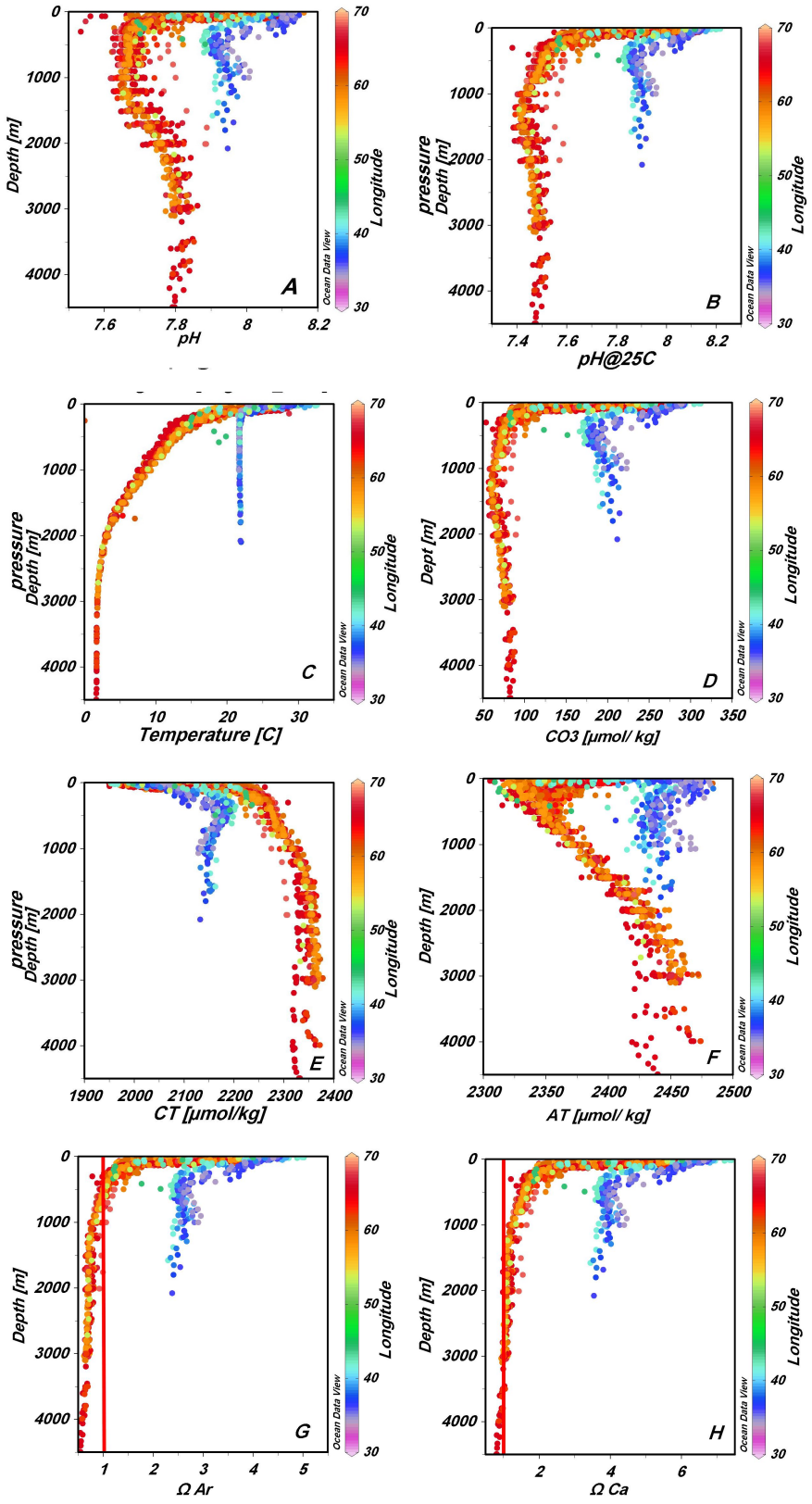

FIGURE 7.12: Vertical distribution of: (A) pH, (B) pH at 25°C, (C) temperature, (D) CO_2^{3-} concentration, (E) C_T, (F) A_T, (G) degree of saturation of aragonite (Ω Ar), and (H) degree of saturation of calcite (Ω Ca) of the Arabian Sea (55°E–70°E) and the Red Sea (30°E–45°E). Longitude is shown as color in Z axis to separate the two regions.

The effect of temperature on pH was determined by holding temperature constant at 25°C and re-computing all pH values. The difference between pH at in situ temperatures and those at 25°C (ΔpH) is plotted against ΔSST (=25-SST) for the surface waters (Figure 7.13). As is shown the slope is about −0.0146 for Arabian Sea and −0.0147 for Red Sea. This can be used to estimate the pH response expected from the anthropogenic 0.5°C warming of the Arabian Sea during 1904–1994 reported by Kumar et al. (2009a). Multiplying the above slope with 0.5 we obtain that the above warming could drive a pH decrease of about 0.007 in the area.

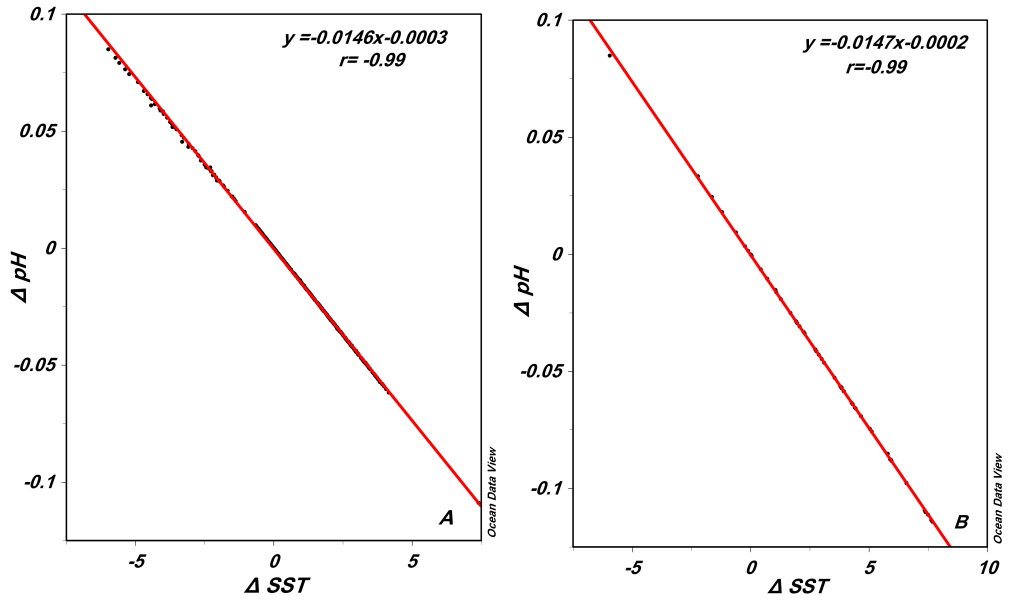

FIGURE 7.13: Δ pH as a function of ΔSST in (A) the Arabian Sea and (B) Red Sea.

Chapter 8

Conclusions and recommendation

The oceanic uptake of anthropogenic CO_2 from the atmosphere is decreasing the pH and lowering the CO_3^{2-} concentration and the degree of the saturation of aragonite and calcite in the upper ocean. These processes, known as ocean acidification, are predicted to decrease oceanic pH by 0.3-0.4 units relative to pre-industrial values by the end of this century (Feely et al., 2009).

Based on available data from the Arabian Sea and Red Sea, spatial and seasonal variations in pH and degree of saturation of aragonite and calcite were studied. The temperature and biology effects control the pH in both seas. During winter the surface average pH, ΩAr, and ΩCa in the Arabian Sea were 8.07±0.01, 3.9±0.1 and 5.9±0.2, respectively. During summer season (southwest monsoon) upwelling along the coast of Oman leads to low values of pH (≈ 7.9), ΩAr (≈ 2.36), and ΩCa (≈ 3.62).

The climate variation driven by the monsoon in the Arabian Sea also affects the south region of the Red Sea, while the north and the central region of the Red Sea are affected by the Mediterranean climate. For the Red Sea, the surface average pH was 8.1±0.02 during winter with higher values in the north due to low temperatures and high A_T and C_T. The ΩAr and ΩCa were around 4.12±0.02 and 6.2±0.15, respectively, with high values in the central due to the high temperatures in this part of the Red Sea. In contrast summer surface pH averaged to 8.07±0.03, with higher values in the north and the south due to the temperature variations.

The summer ΩAr and ΩCa were averaged to 4.6±0.3 and 6.95±0.35, respectively, with higher values in the south and north. This is attributed to the high biological productivity in the south and the high temperature in the center of the Red Sea.

The vertical distributions showed that the Arabian Sea is undersaturated with respect of aragonite and calcite below 600 and 3500 m, respectively, whereas the Red Sea is supersaturated throughout the water column.

During the summer season, the Arabian Sea may give us insights into how ecosystem adapt to high CO_2 levels, by studying the impact of the natural high pH gradients produced by the coastal upwelling system, when mean pH conditions reach values that are similar to those expected for the end of the century. Additionally, global warming seems to be amplifying any acidification resulting from the increase in atmospheric CO_2. Further investigation of these issues and generally the tracking of acidification and its impacts require large-scale, sustained, in situ measurements. New monitoring sites and repeated surveys need to be established in this region.

Bibliography

Abdel Aleem, A., J. R. Morgan, and P. A. Verlaan (2010), Arabian Sea. In Encyclopdia Britannica. Retrieved May 29, 2010, from Encyclopdia Britannica Online: http://www.britannica.com/EBchecked/topic/31653/Arabian-Sea, last visited April 2010.

Ali, E. (2008), The Inorganic Carbon Cycle in the Red Sea, Master's thesis, University of Bergen.

Bates, N. R. (2007), Interannual variability of the oceanic CO_2 sink in the subtropical gyre of the North Atlantic Ocean over the last 2 decades, *Journal of Geophysical Research*, *112*, 27, doi:10.1029/2006JC003759.

Bijma, J., S. Cooley, S. Doney, R. A. Feely, J. P. Gattuso, W. Howard, U. Riebesell, D. Roberts, C. Turley, and others. (2009), Ocean Acidification: The Facts. A special introductory guide for policy advisers and decision makers, *European Project on Ocean Acidification (EPOCA)*, Laffoley, D. dA. and Baxter, J. M, ocean Acidification Reference User Group.

Bradshaw, A. L., P. G. Brewer, and D. K. Shafer (1981), Measurements of total carbon dioxide and alkalinity by potentiometric in the GEOSECS program, *Earth and planetary science letters*, *55*, 99–115.

Brewer, P. G. (1997), Ocean chemistry of the fossil fuel CO_2 signal: the haline signal of "Business as usual", *Geophysical Research Letters*, *24*, 1367–1369.

Caldeira, K., and M. E. Wickett (2003), Oceanography: Anthropogenic carbon and ocean pH, *Nature*, *425*, 365, doi:10.1038/425365a.

Cao, L., and K. Caldeira (2007), Ocean acidification and atmospheric CO_2 stabilization, *Geophysical Research Letters*, *34*(3), doi:10.1029/2006GL028605.

Cao, L., and K. Caldeira (2008), Atmospheric CO_2 stabilization and ocean acidification, *Geophysical Research Letters*, *35*, doi:10.1029/2008GL035072.

Chierici, M., and A. Fransson (2009), Calcium carbonate saturation in the surface water of the Arctic Ocean: undersaturation in freshwater inuenced shelves, *Biogeosciences*, *6*, 2421–2432.

Cochran, J. R. (2002), Red Sea, AccessScience@McGraw-Hill, doi:10.1036/1097--8542.576200.

Cooper, T., G. D. K. Fabricius, and J. Lough (2008), Declining coral calcifcation in massive Porites in two nearshore regions of the northern Great Barrier Reef, *Global Change Biology*, *14*, 529–538.

Dickson, A. G. (1984), pH scales and proton-transfer reactions in saline media such as sea water, *Geochimica Et Cosmochimica Acta, Elsevier.*, *48*(11), 2299–2308, doi:10.1016/0016-7037(84)90225-4.

Dickson, A. G. (1990), Thermodynamics of the dissociation of boric acid in synthetic sea water from 273.15 to 318.15 K, *Deep-sea research*, *37*, 755–766.

Dickson, A. G., C. L. Sabine, and J. R. Christian (2007), Guide to best practices for ocean CO_2 measurements, *Pices Special Publication, 3. North Pacific Marine Science Organization (PICES): Sidney, BC (Canada)*, p. 175 pp.

Dore, J. E., R. Lukas, D. W. Sadler, M. J. Church, and D. M. Karl (2009), Physical and biogeochemical modulation of ocean acidifcation in the central North Pacifc, *Proceedings of the National Academy of Sciences of the United States of America*, *106*, 235–240, doi:10.1073/pnas.0906044106.

Edwareds, F. G. (1987), Climate and oceanography In Red Sea, *Pergamon press, Oxford*, Edwareds, A. J. and Head, S. M.

Elageed, S. (2010), Factor controlling Alkalinity in the Arabian Sea and Red Sea, Master thesis, university of Bergen.

Fabry, V. J., B. Seibel, R. A. Feely, and J. C. Orr (2008), Impacts of ocean acidifcation on marine fauna and ecosystem processes, *ICES Journal of Marine Science*, *65*, 414.

Feely, R. A., C. L. Sabine, K. Lee, W. Berelson, J. Kleypas, V. J. Fabry, and F. J. Millero (2004), Impact of anthropogenic CO_2 on the $CaCO_3$ system in the oceans, *Journal of Science*, *305*, 268–362.

Feely, R. A., S. C. Doney, and S. R. Cooley (2009), Ocean Acidification: Present Conditions and Future Changes in a High-CO_2 world, *Oceanography*, *22*(4).

Field, C. B., M. J. Behrenfield, J. T. Randerson, and P. Falkowski (1998), Primary production of the biosphere: Integrating terrestrial and oceanic components, *Science*, *281*, 237–240.

Flagg, C., and H. Kim (1998), Upper ocean currents in the northern Arabian Sea from shipboard ADCP measurements collected during the 1994–1996 US JGOFS and ONR programs, *Deep-Sea Research Part II*, *45*(10-11), 1917–1959.

Gattuso, J. P., M. Frankignoulle, I. Bourge, R. S., and R. W. Buddemeier (1998), Efect of calcium carbonate saturation of seawater on coral calcication, *Global Planet Change*, *18*, 37–46.

Hansson, I. (1973), A new set of pH-scales and standard buffers for sea water, *Deep Sea Research and Oceanographic Abstracts*, *20*, 479–490.

Henderson, C. (2006), Ocean acidification: the other CO_2 problem, *New Scientist Environment of New Scientist magazine*, *2563*, 28–33.

Honda, M. C., M. Kusakabel, S. Nakabayashil, S. G. Manganini, and S. Honjo (1997), Change in pCO_2 through biological activity in the marginal seas of the western north pacific: The efficiency of the biological pump estimated by a sediment trap experiment, *Journal of oceanography*, *53*, 645–662.

Janzen, H. H. (2004), Carbon cycling in earth systems–a soil science perspective, *Agriculture, Ecosystems & Environment*, *104*, 399–417.

Kleypas, J. A., R. A. Feely, V. J. Fabry, C. Langdon, C. L. Sabine, and L. L. Robbins (2006), Impacts of Ocean Acidication on Coral Reefs and Other Marine

Calciers: A Guide for Future Research, *report of a workshop 88pp*, sponsored by NSF, NOAA, and the U.S. Geological Survey, St. Petersburg, FL.

Kumar, S., R. P. Roshin, J. Narvekar, P. K. Dinesh Kumar, and E. Vivekanandan (2009a), Response of the Arabian Sea to global warming and associated regional climate shift, *Marine Environmental Research*, *68*, 217–222.

Kumar, S. P., S. Sardesai, and N. Ramaiah (2009b), A decade of physical and biogeochemical measurements in the northern Indian Ocean, *National Institute of Oceanography, Dona Pula, India*, pp. 400–403.

Lee, C. M., B. H. Jones, K. H. Brink, and A. S. Fischer (2000), The upper-ocean response to monsoonal forcing in the Arabian Sea: seasonal and spatial variability, *Deep Sea Research*, *47*, 1177–1226.

Lewis, E., and D. W. R. Wallace (1998), *Program Developed for CO_2 System Calculations*, ORNL/CDIAC-105, Carbon Dioxide Information Analysis Center, Oak Ridge National Laboratory, U.S. Department of Energy, Oak Ridge, Tennessee.

Maillard, C., and G. Soliman (1986), Hydrography of the Red Sea and exchanges with the Gulf of Aden in summer, *Oceanography*, *93*, 249–269.

Mehrbach, C., C. H. Culberson, J. E. Hawley, and R. M. Pytkowicz (1973), Measurement of the apparent dissociation constants of carbonic acid in seawater at atmospheric pressure, *Limnology and Oceanography*, *18*, 897–907.

Millero, F., E. Degler, D. OSullivan, C. Goyet, and G. Eischeid (1998), The carbon dioxide system in the Arabian Sea, *Deep-Sea research II*, *45*, 2225–2252.

Moel, H. D., G. M. Ganssen, F. G. C. Peeters, S. J. A. Jung, D. Kroon, G. J. A. Brummer, and R. E. Zeebe (2009), Planktic foraminiferal shell thinning in the Arabian Sea due to anthropogenic ocean acidication, *Biogeosciences*, *6*, 1917–1925.

Morcos, S. A. (1970), Physical and chemical oceanography of the Red Sea, *Oceanography and Marine Biology Annual Review*, *8*, 73–202.

Morrison, J. M. (1997), Inter-monsoonal changes in the T-S properties of the near surface waters of the Northern Arabian Sea, *Geophysical Research Letters*, *24(21)*, 2553–2556.

Moy, A. D., W. R. Howard, S. G. Bray, and T. W. Trull (2009), Reduced calcification in modern Southern Ocean planktonic foraminifera, *Nature Geoscience*, *2*, 276–280, doi:10.1038/NGEO46.

Murray, S. P., and W. Johns (1997), Direct observations of seasonal exchange through the Bab el Mandab Strait, *Geophysical Research Letter.*, *24(21)*, 2557–2560.

Orr, J. C., V. J. Fabry, O. Aumont, L. Bopp, S. C. Doney, R. A. Feely, A. Gnanadesikan, N. Gruber, A. Ishida, F. Joos, R. M. Key, K. Lindsay, E. Maier-Reimer, R. Matear, P. Monfray, A. Mouchet, R. J. Najjar, G. Plattner, K. B. Rodgers, C. L. Sabine, J. L. Sarmiento, R. Schlitzer, R. D. Slater, I. J. Totterdell, M. Weirig, Y. Y., and A. Yool (2005), Anthropogenic ocean acidification over the twenty-first century and its impact on calcifying organisms, *Nature*, *437(7059)*, 681–686, doi:10.1038/nature04095.

Papaud, A., and A. Poisson (1986), Distribution of dissolved CO_2 in the Red Sea and correlation with other geochemical tracers, *Jornal of Marine Research*, *44*, 385–402.

Patzer, W. C. (1974), Wind-induced reversal in the Red Sea circulation, *Deep Sea Research*, *21*, 109–121.

PERSGA (1998), *Strategic Action Program for the Red Sea and Gulf of Aden.*

Raven, J., K. Caldeira, H. Elderfield, O. Hoegh-Guldberg, P. Liss, U. Riebesell, J. Shepherd, C. Turley, A. Watson, R. Heap, R.and Banes, and R. Quinn (2005), Ocean acidification due to increasing atmospheric carbon dioxide, *Tech. rep.*, The Royal Society, Working Group.

Riebesell, U., U. Zondervan, I. Rost, B. Tortell, D. Philippe, R. E. Zeebe, and F. M. M. Morel (2000), Reduced calcification of marine plankton in response to increased atmospheric CO_2, *Nature*, *407*, 364–367, doi:10.1038/35030078.

Roberts, J. M. D., W. R. Howard, A. D. Moy, J. L. Roberts, T. W. Trull, S. G. Bray, and R. R. Hopcrof (2008), Interannual variability of pteropod shell weights in the high-CO_2 Southern Ocean, *Biogeosciences Discussions*, *5:4*, 453–480.

Sarmiento, J., and N. Gruber (2006), *Ocean biogeochemical dynamics*, Princeton University Press.

Smeed, D. A. (1997), Seasonal Variation of the flow in the strait of Bab el Mandab, *Oceanography*, *206*, 773–781.

Sofianos, S. S., and W. E. Johns (2003), An Oceanic General Circulation Model (OGCM) investigation of the Red Sea circulation: 2. Three-dimensional circulation in the Red Sea, *Journal of Geophysical Research*, *108(C3)*, 3066, doi: 10.1029/2001JC001185.

Sofianos, S. S., W. E. Johns, and S. P. Murray (2002), Heat and freshwater budgets in The Red Sea from direct observations at Bab el Mandeb, *Deep Sea Research*.

Souvermezoglou, T., N. Metzel, and A. Poisson (1989), Red Sea budgets of salinity, nutrients and carbon calculated in the Strait of Bab Al Mandab during summer and winter seasons, *Journal of Marine Research*, *47*, 441–456.

Tomczak, M., and J. Godfrey (2001), Regional oceanography: an introduction, Oxford.

Tomczak, M., and J. S. Godfrey (2003), *Regional oceanography: an introduction*, 2nd edition ed., 390 pp., Daya Publishing House, pdf version 1.1 (December2006).

Turley, C. (2005), Impacts of Ocean Acidification on Coral Reefs and Other Marine Calcifiers: A Guide for Future Research, *Tech. rep.*, report of a workshop in 18–20 April.

Turley, C., J. Blackford, S. Widdicombe, D. Lowe, P. D. Nightingale, and A. B. Rees (2006), *Reviewing the impact of increased atmospheric CO_2 on oceanic pH and the marine ecosystem. In: Avoiding Dangerous Climate Change*, Cambridge University Press.

Turley, C., J. M. Roberts, and J. M. Guinotte (2007), Perspective: Corals in deep-water: Will the unseen hand of ocean acidification destroy cold-water ecosystems?, *Coral Reefs*, *26*, 445–448.

UNEP (1997), Assessment of Land-based Sources and Activities Affecting the Marine Environment in the Red Sea and Gulf of Aden, *Tech. Rep. 166*, UNEP Regional Seas Reports and Studies.

Vitousek, P. M., H. A. Mooney, J. Lubchenco, and J. M. Melillo (2008), *Urban Ecology. Chapter 1: Human Domination of Earth's Ecosystems*, 3-13 pp., Springer US.

Weiss, R. F. (1974), Carbon dioxide in water and sea water: the solubility of a non-ideal gas, *Marine Chemistry*, *2*, 203–215.

Wentworth, J. (2009), Ocean acidification,, *parliamentary office of science and technology (POSTnote)*, *343*(343).

Werner, F., and K. Lange (1975), Bathymetric Survey of the Sill Area between the Red Sea and the Gulf of Aden, *Geol. Jahrb*, *13*, 125–130.

Zeebe, R. E., and . Wolf-Gladrow, D. . (2001), *CO_2 in seawater: equilibrium, kinetics, isotopes*, 1, 1–83 pp., Elsevier Oceanography Series, Elsevier: Amsterdam.